Cell Reports

Article

Adipose TGFβ-asprosin memory promotes obesity relapse and offspring obesity susceptibility

Graphical abstract

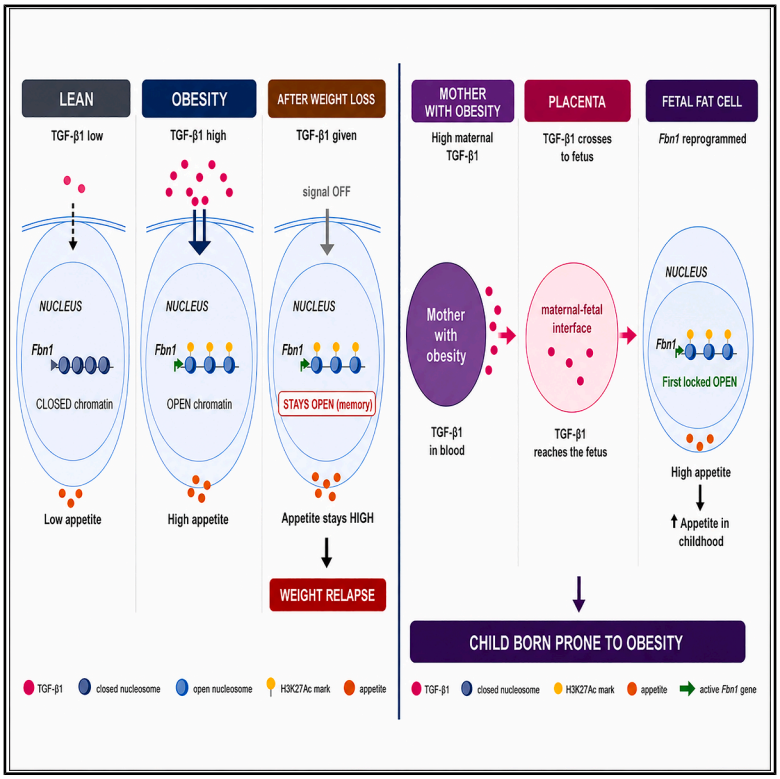

Highlights

- TGF-β1 induces a persistent adipose transcriptional memory
- Sustained asprosin elevation promotes obesity relapse after weight loss
- Maternal TGF-β1 increases offspring susceptibility to diet-induced obesity
- Blocking the TGF-β1-asprosin-Ptprd axis prevents relapse and offspring obesity

Authors

Brian C. Kim, Hiba Obeid, Yi Fan Chen, ..., Ila Mishra, Seth Field, Atul R. Chopra

Correspondence

atul.chopra@case.edu

In brief

Kim et al. show that obesity-associated TGF-β1 establishes a persistent adipocyte transcriptional memory that sustains asprosin production. In mice, this persistent hormonal state promotes weight regain after weight loss and increases offspring susceptibility to obesity, identifying the TGF-β1-asprosin-Ptprd axis as a potential therapeutic target.

Kim et al., 2026, Cell Reports *45*, 117809
August 25, 2026
https://doi.org/10.1016/j.celrep.2026.117809

CellPress

Cell Reports

CellPress
OPEN ACCESS

Article

Adipose TGFβ-asprosin memory promotes obesity relapse and offspring obesity susceptibility

Brian C. Kim,[1] Hiba Obeid,[1] Yi Fan Chen,[1] Christopher Kim,[2] Adam Lieberman,[2] Bijoya Basu,[1] Elizabeth S. Silva,[2] Jingzhi Meng,[2] Kyle Starost,[2] Natalia Aladyshkina,[2] Ila Mishra,[2,3,4] Seth Field,[2] and Atul R. Chopra[1,2,5,6,*]

[1]Department of Genetics and Genome Sciences, Case Western Reserve University, Cleveland, OH, USA
[2]Harrington Discovery Institute, University Hospitals Cleveland Medical Center, Cleveland, OH, USA
[3]Division of Endocrinology, Diabetes and Metabolism, Department of Internal Medicine, College of Medicine, University of Kentucky, Lexington, KY, USA
[4]Department of Physiology, College of Medicine, University of Kentucky, Lexington, KY, USA
[5]Department of Medicine, University Hospitals Cleveland Medical Center, Cleveland, OH, USA
[6]Lead contact
*Correspondence: atul.chopra@case.edu
https://doi.org/10.1016/j.celrep.2026.117809

SUMMARY

Obesity is associated with frequent relapse after weight loss and increased obesity risk in offspring of mothers with obesity, but the mechanisms underlying this persistence remain incompletely understood. We find that obesity-elevated cytokine TGF-β1 activates fibrillin-1 (*Fbn1*) transcription in adipocytes, increasing production of the appetite-stimulating hormone asprosin. Transient exposure to elevated TGF-β1 remodels chromatin at the *Fbn1* locus, generating a durable transcriptional state associated with sustained *Fbn1* expression and plasma asprosin elevation after weight loss and normalization of TGF-β1. In mouse models, this persistent asprosin elevation increases food intake, promoting weight regain. In parallel, maternal TGF-β1 exposure during gestation programs offspring adipose tissue, leading to persistent *Fbn1* expression, elevated plasma asprosin, and increased susceptibility to diet-induced obesity. Finally, genetic or pharmacologic disruption of the *Fbn1*-asprosin-Ptprd axis prevents both phenomena. These findings identify an adipose TGF-β1-asprosin pathway that constitutes a memory of prior obesity and promotes obesity relapse and intergenerational obesity susceptibility.

INTRODUCTION

Obesity is distinguished not only by excess adiposity but by its remarkable persistence.[1] Most individuals who achieve weight loss ultimately regain it, irrespective of the intervention used.[2,3] This near-universal relapse suggests that obesity induces durable biological changes that persist beyond weight reduction. The same persistence extends across generations: maternal obesity markedly increases the risk of obesity in offspring, independent of shared diet or environment.[4–12] Together, these phenomena—relapse and inheritance—imply that obesity leaves behind a molecular imprint that stabilizes its own recurrence, yet the nature of this imprint remains unknown.

Among adipose-derived endocrine factors, asprosin has emerged as a potent hormonal signal elevated in obesity.[13] Asprosin is generated by C-terminal cleavage of fibrillin-1 (*Fbn1*), secreted primarily from white adipose tissue (WAT), and acts on Ptprd-expressing AgRP neurons in the hypothalamus to increase neuronal excitability and stimulate appetite.[14–17] Circulating asprosin correlates with body weight and insulin resistance, and inhibition of either asprosin or Ptprd ameliorates hyperphagia and metabolic dysfunction in mice.[18–21] Despite these insights, the molecular mechanism by which obesity increases *Fbn1* expression and raises circulating asprosin remains undefined.

We sought to identify the upstream signals that activate *Fbn1* transcription in adipocytes and drive excess asprosin production in obesity. In the course of this effort, we uncovered an unexpected link between an obesity-associated cytokine and persistent chromatin remodeling at the *Fbn1* locus. What began as an attempt to understand how obesity elevates asprosin revealed a molecular explanation for two defining features of the disease—its relapse after weight loss and its transmission to offspring.

These findings identify a unifying process in which transient inflammatory signaling establishes a stable transcriptional state that sustains adipose endocrine output. This mechanism provides a coherent molecular basis for the long-standing paradox of obesity's permanence, connecting relapse and inheritance through a single, durable modification of adipose gene regulation.

RESULTS

TGF-β1 drives transcriptional activation of *Fbn1* in adipocytes through canonical signaling

We previously established that *Fbn1* mRNA is elevated in the WAT of mice with obesity, correlating with increased plasma asprosin

levels.[16] We confirmed this in mice with diet-induced obesity (DIO) across both visceral and subcutaneous fat depots (Figure S1A). To identify the obesity-associated signal driving *Fbn1* transcription, we screened key cytokines known to be elevated in obesity.[22–24] Among them, TGF-β1 emerged as a potent enhancer, significantly increasing *Fbn1* mRNA (Figures 1A and S1B) and media asprosin (Figure 1B) in differentiated adipocytes (3T3-L1 cells). We validated this *in vivo* by injecting recombinant TGF-β1 intraperitoneally (i.p.) in wild-type (WT) mice, which led to elevated *Smad7* mRNA in WAT, confirming TGF-β1 signaling activation (Figure S1C).[25] This also increased *Fbn1* mRNA in both visceral and subcutaneous fat depots (Figure 1C), a finding consistent in female mice, eliminating sexual dimorphism as a consideration (Figures S1D and S1E). To determine whether TGF-β1 actively regulates *Fbn1* transcription, we performed quantitative PCR (qPCR) on CUT&RUN[26] isolated DNA from 3T3-L1 cells, probing for RNA polymerase II occupancy at the *Fbn1* locus. TGF-β1 exposure resulted in increased RNA polymerase II occupancy at the *Fbn1* locus, indicating active transcription (Figure S1F). To determine whether transcription is the predominant process for TGF-β1-mediated asprosin production by adipocytes, we exposed differentiated 3T3-L1 cells to actinomycin D to block RNA transcription. This resulted in complete inhibition of TGF-β1-induced media asprosin accumulation (Figure S1G), underscoring the necessity of RNA transcription in this process.

Asprosin is encoded within the penultimate and ultimate exons of *Fbn1*, raising the possibility that it could be produced from a distinct transcript separate from *Fbn1*.[16] To explore this, we examined CAGE analysis from the FANTOM5 database,[27] which identified a single transcription start site (TSS) and a single CpG island for the entire *FBN1* gene (Figure S1H). We also tested whether TGF-β1 exposure led to greater accumulation of mRNA specific to the asprosin coding region compared with the rest of the *Fbn1* locus. Results showed no additional elevation of asprosin-coding mRNA beyond the rest of *Fbn1* mRNA, suggesting the absence of asprosin-specific transcriptional regulation by TGF-β1 (Figure S1I).

TGF-β1 signaling begins when the ligand binds to the TGF-β type II receptor, which then dimerizes with the type I receptor, activating downstream pathways.[28] Several transcription factors, as well as the coactivator Smad4, are essential canonical components of this pathway.[29] To determine whether TGF-β1 activates *Fbn1* transcription through its canonical signaling pathway, we silenced *Tgfbr2* in 3T3-L1 cells. Knockdown of *Tgfbr2* markedly blunted the TGF-β1-induced increase in both *Fbn1* and *Smad7* mRNA levels (Figures 1D and 1E). Likewise, *Smad4* knockdown produced a similar suppression (Figures 1F and 1G), demonstrating that canonical TGF-β1 signaling is essential for *Fbn1* transcription.

TGF-β1 has been consistently found to be elevated in obesity, both in animal and human studies.[24,30] Pharmacologic inhibition of TGF-β1 in obesity improves body weight and glucose tolerance, implicating TGF-β1 as a causal factor.[24] To determine whether asprosin is essential for TGF-β1-mediated obesity, we used the $Fbn1^{NPS/+}$ mice, which exhibit a deficiency in plasma asprosin.[13] WT mice treated with recombinant TGF-β1 gained weight, while $Fbn1^{NPS/+}$ mice did not, indicating that asprosin is necessary for TGF-β1-driven weight gain (Figures 1H and S1J).

TGF-β1 also regulates gene expression by remodeling chromatin through histone acetylation via p300/CBP activation.[31–33] To test whether this mechanism is necessary for TGF-β1-mediated *Fbn1* transcription, we treated TGF-β1-stimulated cells with A-485, a potent p300/CBP inhibitor. We found that it effectively blocked TGF-β1-induced *Fbn1* overexpression without affecting *Smad7* overexpression (Figures S1K and S1L). This demonstrates that p300/CBP HAT activity is crucial for TGF-β1-induced *Fbn1* transcription but is dispensable for *Smad7*, highlighting locus-specific differences in TGF-β1-driven chromatin remodeling and gene expression. Together, these findings identify TGF-β1 as a key obesity-associated factor that activates *Fbn1* transcription through canonical *Smad4* signaling and p300/CBP activity, thereby driving asprosin production and weight gain.

TGF-β1 exposure induces a lasting increase in *Fbn1* transcription and plasma asprosin

During our studies, we discovered a surprising persistence in TGF-β1-induced *Fbn1* mRNA elevation long after TGF-β1 signaling had ceased. When 3T3-L1 cells were exposed to recombinant TGF-β1 for 4 days and then maintained in TGF-β1-free media for an additional 14 days, both *Fbn1* mRNA and media asprosin levels remained significantly elevated (Figures 2A and 2B). In contrast, *Smad7* mRNA, a classical TGF-β1 target, rapidly returned to baseline (Figure 2C), revealing distinct regulatory kinetics for *Fbn1* and *Smad7*. To test whether the persistence of *Fbn1* elevation resulted from altered mRNA stability, we measured *Fbn1* transcript half-life following TGF-β1 exposure in the presence of actinomycin D. The half-life of *Fbn1* mRNA was 18.5 h, far too short to account for the prolonged elevation observed (Figure 2D), suggesting that TGF-β1 triggers a lasting transcriptional program rather than sustained signaling or mRNA stabilization.

To test whether this occurs *in vivo*, WT mice were injected with recombinant TGF-β1 or PBS twice daily for 4 days, followed by a 14-day recovery without intervention. Because the circulating half-life of active TGF-β1 is only 2–3 min,[34] no residual TGF-β1 was detectable after this period (Figure 2E). Nevertheless, *Fbn1* mRNA and plasma asprosin remained markedly elevated 14 days after treatment (Figures 2F–2H), while white adipose *Smad7* mRNA and other orexigenic signals such as NPY and ghrelin were unchanged (Figures 2I, S2A, and S2B).

Given that TGF-β1-induced increases in adipose *Fbn1* and plasma asprosin persist for weeks, we next asked whether this brief cytokine pulse leaves a lasting metabolic imprint. Indeed, mice exposed to TGF-β1 2 weeks earlier displayed accelerated weight gain when challenged with a high-fat diet (HFD), an effect completely abolished by asprosin blockade (Figures 2J and S2C).

Together, these findings reveal that obesity-associated TGF-β1 signaling produces long-lasting transcriptional activation of *Fbn1* in adipose tissue, leading to persistently elevated plasma asprosin and a durable shift in metabolic state. These sustained effects suggest that TGF-β1, at the magnitude and duration associated with obesity, imprints a molecular memory within adipocytes, enabling prolonged hormone production long after signaling has ceased.

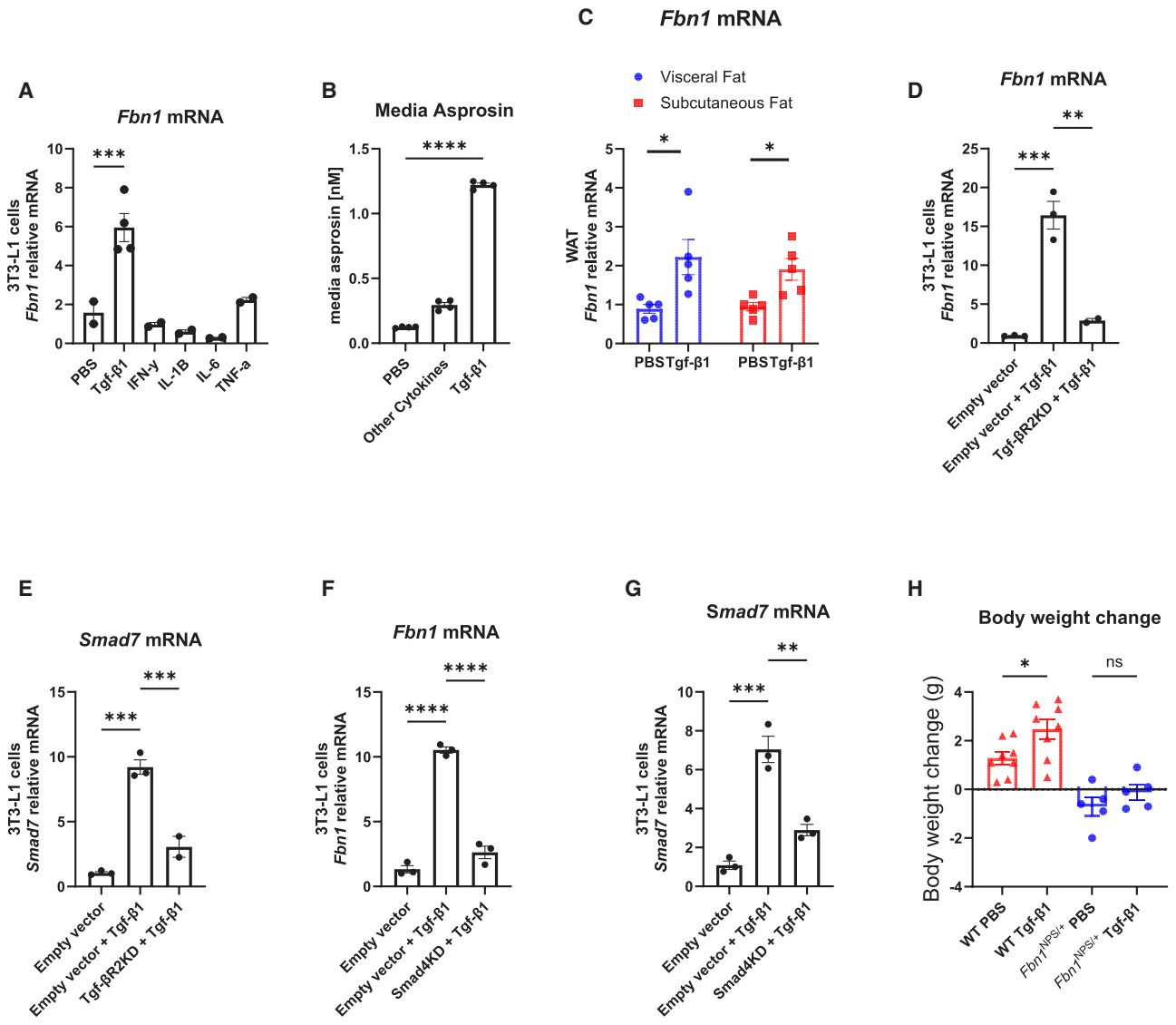

Figure 1. TGF-β1 activates *Fbn1* transcription in white adipose tissue

(A) qPCR showing relative mRNA levels of *Fbn1* in differentiated 3T3-L1 cells exposed to 20 ng/mL of the indicated cytokines for 48 h ($n = 2$ for PBS, IFN-γ, IL-1β, IL-6, and TNF-α; $n = 4$ for TGF-β1).

(B) Media asprosin detection with sandwich ELISA of differentiated 3T3-L1 cells exposed to PBS (control), 20 ng/mL of TGF-β1, or a cocktail of other cytokines (IFN-γ, IL-1β, IL-6, and TNF-α) for 48 h ($n = 4$ per group).

(C) qPCR showing relative mRNA levels of *Fbn1* in visceral (perigonadal) and subcutaneous (back) adipose tissue depots after 2 i.p. injection of PBS or 0.5 μg TGF-β1 spaced 6 h apart in 12-week-old male C57BL/6 mice ($n = 5$ per group).

(D and E) qPCR showing relative mRNA levels of *Fbn1* and *Smad7* (respectively) of differentiated 3T3-L1 cells with knockdown of *Tgfbr2* utilizing pLKO.1 lentivirus and addition of 20 ng/mL TGF-β1 for 48 h ($n = 3$ for control and control + TGF-β1 and $n = 2$ for *Tgfbr2* KD + TGF-β1).

(F and G) qPCR showing relative mRNA levels of *Fbn1* and *Smad7* (respectively) of differentiated 3T3-L1 cells with knockdown of *Smad4* utilizing pLKO.1 lentivirus and addition of 20 ng/mL TGF-β1 for 48 h ($n = 3$ for all groups).

(H) Five-day body weight change of 12-week-old male *Fbn1*$^{NPS/+}$ mice maintained on *ad libitum* HFD that received 2 days of i.p. injections, twice a day of PBS or 0.5 μg of TGF-β1 ($n = 6$ for WT TGF-β1 and $n = 5$ for all other groups).

Error bars represent mean ± SEM. *$p < 0.05$, **$p < 0.01$, ***$p < 0.001$, and ****$p < 0.0001$ by one-way ANOVA (A–H).

Independent replication confirms TGF-β1-driven persistent *Fbn1* upregulation

To ensure the robustness of our findings, the results were reproduced in an independent laboratory following the same protocol. In differentiated 3T3-L1 adipocytes treated with TGF-β1 for 4 days, followed by a 2-week withdrawal period, it was confirmed that *Fbn1* mRNA remained significantly elevated while *Smad7* expression returned to baseline levels, precisely recapitulating the original findings (Figures S3A and S3B). Importantly, an additional PBS-treated control maintained for

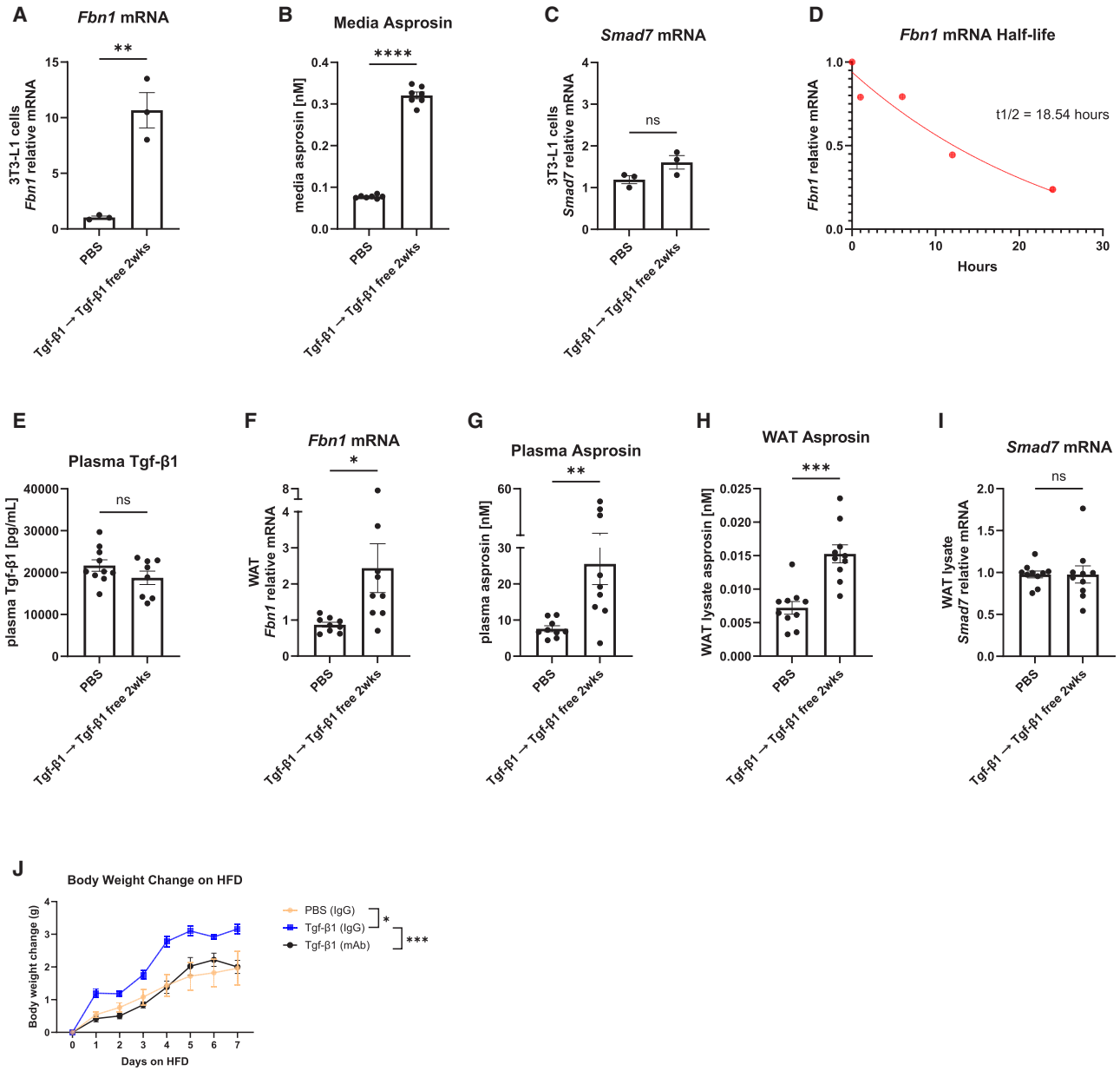

Figure 2. TGF-β1 causes persistent elevation of white adipose *Fbn1* mRNA and plasma asprosin

(A) qPCR showing relative mRNA levels of *Fbn1* in differentiated 3T3-L1 cells after addition of PBS or 20 ng/mL TGF-β1 media for 4 days followed by TGF-β1-free media for 14 days (n = 3 per group).

(B) Media asprosin detection with sandwich ELISA of differentiated 3T3-L1 cells exposed to PBS or 20 ng/mL TGF-β1 media for 4 days followed by TGF-β1-free media for 14 days (n = 7 per group).

(C) qPCR showing relative mRNA level of *Smad7* in differentiated 3T3-L1 cells after addition of PBS or 20 ng/mL TGF-β1 media for 4 days followed by TGF-β1-free media for 14 days (n = 3 per group).

(D) mRNA half-life showing relative abundance of *Fbn1* mRNA after addition of 30 μg/mL actinomycin D and 20 ng/mL TGF-β1. mRNA was sampled at multiple time points, and half-life was determined using a one-phase decay non-linear fit.

(E) Mouse plasma sandwich ELISA for total TGF-β1 in 12-week-old male WT C57BL/6 mice after 4 days of 2 daily injections of PBS or 0.5 μg TGF-β1, followed by 14 days without intervention (n = 10 for PBS group and n = 8 for TGF-β1 group).

(F) qPCR showing relative mRNA level of *Fbn1* in visceral white adipose tissue in 12-week-old male WT C57BL/6 mice after 4 days of 2 daily injections of PBS or 0.5 μg TGF-β1, followed by 14 days without intervention (n = 9 for all groups).

(G) Mouse plasma sandwich ELISA for asprosin in 12-week-old male WT C57BL/6 mice after 4 days of 2 daily injections of PBS or 0.5 μg TGF-β1 followed by 14 days without intervention (n = 9 for all groups).

(legend continued on next page)

2 weeks demonstrated that prolonged incubation alone does not affect *Fbn1* or *Smad7* transcript levels. In parallel, WT C57BL/6J mice injected with TGF-β1 for 4 days and left untreated for an additional 2 weeks showed persistently elevated *Fbn1* mRNA in visceral adipose tissue while *Smad7* levels returned to those of PBS-injected controls (Figures S3C and S3D). Together, these externally reproduced findings confirm that the selective and durable transcriptional upregulation of *Fbn1* following transient TGF-β1 exposure is a robust biological phenomenon that is reproducible across independent laboratories.

TGF-β1 elicits a durable transcriptional program enriched for extracellular matrix genes

To define the full scope of transcriptional alterations triggered by TGF-β1, we performed RNA sequencing under three conditions: differentiated 3T3-L1 adipocytes treated with PBS (condition A), treated with TGF-β1 for 4 days (condition B), and treated with TGF-β1 for 4 days followed by a 14-day period in TGF-β1-free media (condition C) (Figure 3A). Comparing condition A with condition B, Gene Ontology analysis of upregulated transcripts revealed strong enrichment for extracellular matrix (ECM) organization pathways, prominently including *Fbn1* (Figures 3B and 3C).

To characterize gene expression dynamics following TGF-β1 withdrawal, we performed hierarchical tree clustering across all three conditions. Two distinct response patterns emerged. The first group, exemplified by classical TGF-β1 target genes such as *Smad7* and *Skil*, displayed transient induction that subsided after TGF-β1 removal. The second group, which included *Fbn1*, maintained elevated expression even after 14 days in TGF-β1-free media (Figure 3D).

Among the 85 TGF-β1-induced ECM genes, approximately 75% including *Fbn1* remained elevated after TGF-β1 withdrawal, whereas 25% returned to baseline (Figure 3E). Focusing on the genes that sustained their expression post-withdrawal, Gene Ontology analysis again highlighted strong enrichment for ECM-organization pathways (Figure 3F). To quantify persistence across the transcriptome, we ranked all genes that remained upregulated after TGF-β1 removal based on a composite fold-change score incorporating both effect size and significance. *Fbn1* ranked 16th among 878 persistently elevated genes (Figure 3G), with higher-ranked genes including other ECM components, adaptor proteins, cytokines, and protease inhibitors (Table S1).

Together, these findings demonstrate that transient TGF-β1 exposure elicits a broad and durable transcriptional program in adipocytes, characterized by sustained upregulation of ECM-related genes, with *Fbn1* emerging as a central and long-lasting target of TGF-β1 signaling.

TGF-β1 remodels chromatin to sustain *Fbn1* activation and asprosin production

TGF-β1 is a key player in chromatin remodeling, but its impact on the adipose tissue epigenetic landscape remains largely unexplored.[25] Given the persistent elevation of *Fbn1* expression following TGF-β1 exposure, we hypothesized that TGF-β1 might induce long-lasting chromatin accessibility at the *Fbn1* locus. To test this, we performed ATAC-seq[35] on 3T3-L1 cells treated with vehicle (PBS), or exposed to TGF-β1 for 4 days, or exposed to TGF-β1 for 4 days followed by 14 days in TGF-β1-free media (Figure 4A). Gene Ontology analysis of the genes that mapped to peaks significantly elevated in TGF-β1-treated cells was enriched for terms such as "extracellular matrix organization" (Figure 4B). Notably, many chromatin peaks that increased at least 4-fold with TGF-β1 treatment, including those at the *Fbn1* locus, remained elevated above vehicle control even after 14 days in TGF-β1-free media (Figure 4C).

We next referenced our RNA-seq results in 3T3-L1 cells to identify specific ATAC-seq peaks that might explain how TGF-β1-induced chromatin changes drive *Fbn1* transcription. At the *Fbn1* locus, TGF-β1 induced open chromatin peaks downstream of the gene (region 1) and upstream of the TSS (region 2), which persisted even after prolonged TGF-β1 withdrawal (Figure 4D). These loci detected on ATAC-seq in our study were precisely aligned with H3K27ac marks identified previously,[36] suggesting that these loci may be functional enhancers or promoters (Figure S4A). In contrast, TGF-β1-induced open chromatin peaks at the *Smad7* locus regressed to baseline after TGF-β1 withdrawal, consistent with a more transient response (Figure 4E).

Because TGF-β-mediated *Fbn1* transcription depended on histone acetyltransferase activity (Figures S1K–S1L) and its chromatin accessibility coincided with known H3K27ac marks, we next tested whether histone deacetylation following TGF-β1 exposure would suppress its expression. Treatment with ITSA-1, a pan-HDAC activator, significantly reduced *Fbn1* transcript levels and asprosin secretion (Figures 4F and 4G), whereas *Smad7* expression remained unchanged (Figure S4B). These results support the conclusion that TGF-β1 establishes persistent chromatin accessibility at the *Fbn1* enhancer that remains unchanged despite cessation of TGF-β signaling, driving long-term transcriptional upregulation and sustained plasma asprosin levels.

Persistent asprosin elevation drives obesity relapse

Clinical and metabolic studies demonstrate that after weight loss, appetite remains chronically elevated compared with individuals without prior obesity, reflecting a durable biological adaptation that favors weight regain.[37] This persistent hunger drive contributes to obesity's near-universal relapse after weight reduction,[2,3] yet its molecular basis remains unclear. Because transient TGF-β1 exposure induces long-lasting *Fbn1*

(H) Visceral adipose tissue lysate sandwich ELISA for asprosin in 12-week-old-male WT C57BL/6 mice after 4 days of 2 daily injections of PBS or 0.5 μg TGF-β1 followed by 14 days without intervention (n = 10 per group).
(I) qPCR showing relative mRNA level of *Smad7* in visceral white adipose tissue in 12-week-old-male WT C57BL/6 mice after 4 days of 2 daily injections of PBS or 0.5 μg TGF-β1, followed by 14 days without intervention (n = 10 for all groups).
(J) Body weight change of mice from (E)–(H) placed on HFD and treated with daily i.p. injections of IgG or anti-asprosin monoclonal antibody (5.55 μg/g mouse) (n = 5 for all groups). We did not include a PBS (mAb) group, as we have previously shown the mAb has no effect on body weight on lean mice (Figure S6E).
Error bars represent mean ± SEM. *p < 0.05, **p < 0.01, ***p < 0.001, and ****p < 0.0001 by unpaired two-sided t test (A–I) and two-way ANOVA (J).

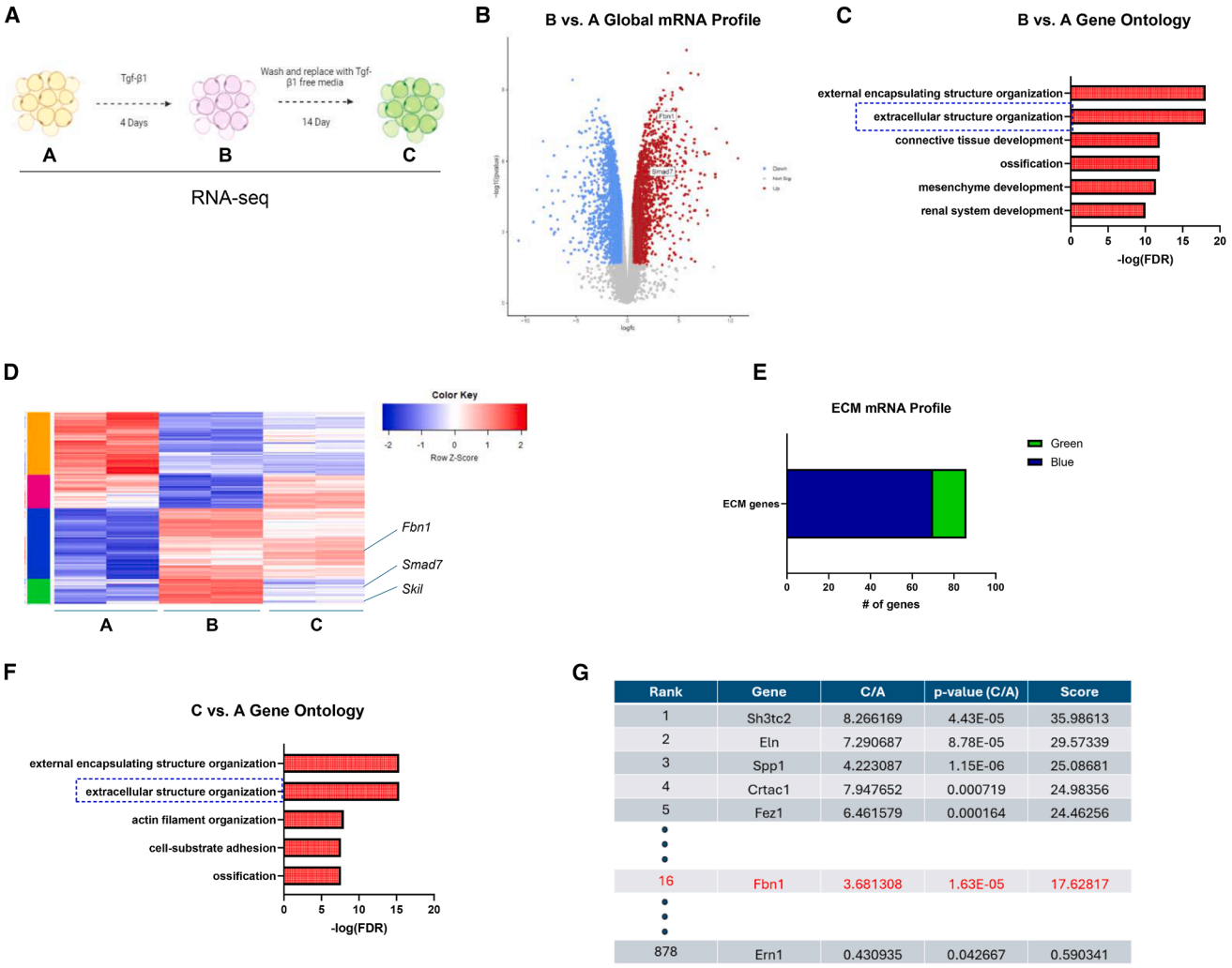

G

Rank	Gene	C/A	p-value (C/A)	Score
1	Sh3tc2	8.266169	4.43E-05	35.98613
2	Eln	7.290687	8.78E-05	29.57339
3	Spp1	4.223087	1.15E-06	25.08681
4	Crtac1	7.947652	0.000719	24.98356
5	Fez1	6.461579	0.000164	24.46256
•				
•				
•				
16	Fbn1	3.681308	1.63E-05	17.62817
•				
•				
•				
878	Ern1	0.430935	0.042667	0.590341

Figure 3. TGF-β1 produces global transcriptomic changes in adipocytes

(A–C) Schematic showing three experimental conditions for RNA-seq: (A) PBS, (B) TGF-β1 for 4 days, and (C) TGF-β1 for 4 days followed by 14 days in TGF-β1-free media. (B) Volcano plot of RNA-sequencing data comparing PBS vs. TGF-β1-treated-differentiated 3T3-L1 cells (A vs. B). Locations of *Fbn1* and *Smad7* are highlighted. (C) Gene Ontology (GO) analysis of upregulated genes after exposure to TGF-β1 in differentiated 3T3-L1 cells.

(D) Hierarchical tree clustering of RNA-sequencing data identifying four distinct gene expression clusters in response to TGF-β1 treatment and withdrawal. Genes were grouped into four clusters based on temporal expression patterns: (orange) downregulated upon TGF-β1 addition and remaining suppressed after withdrawal; (pink) downregulated upon TGF-β1 addition but upregulated after withdrawal; (blue) upregulated upon TGF-β1 addition and remaining elevated after withdrawal; and (green) upregulated upon TGF-β1 addition but downregulated after withdrawal. *Fbn1* is classified within the blue cluster, whereas *Smad7* and *Skil* fall within the green cluster.

(E) Number of extracellular matrix (ECM) genes that belong to the blue and green clusters shown in (D).

(F) Gene Ontology (GO) analysis of upregulated genes after exposure to TGF-β1 and subsequent TGF-β1 withdrawal in differentiated 3T3-L1 cells.

(G) Table showing select genes in blue group of genes for condition C where expression is high after TGF-β1 addition and withdrawal and significantly different compared with control (condition A). Number under C/A column shows log(FC). Score was determined using the following equation: $score = C/A^{*} - log(C/A p\text{-}value)$.

transcription and elevated plasma asprosin (an appetite-stimulating signal), we hypothesized that this pathway encodes a molecular memory of prior obesity that directly contributes to relapse. To test this, we developed two complementary mouse models to assess whether TGF-β1-induced asprosin elevation is both sufficient and necessary for weight regain.

In the first model, DIO mice underwent alternate-day fasting on a chow diet for 14 days (Figure 5A). This regimen reduced body weight by 10% and lowered plasma TGF-β1, but *Fbn1* mRNA, adipose asprosin, and plasma asprosin levels remained elevated (Figures 5B–5E, S5A, and S5B). When maintained on chow or switched to an HFD, these mice regained significantly more weight than age- and sex-matched controls without prior obesity (Figures S5C–S5F). Mice with prior obesity also consumed more food, shifting energy balance toward regain (Figure S5G). *Fbn1* mRNA and plasma asprosin levels strongly correlated with

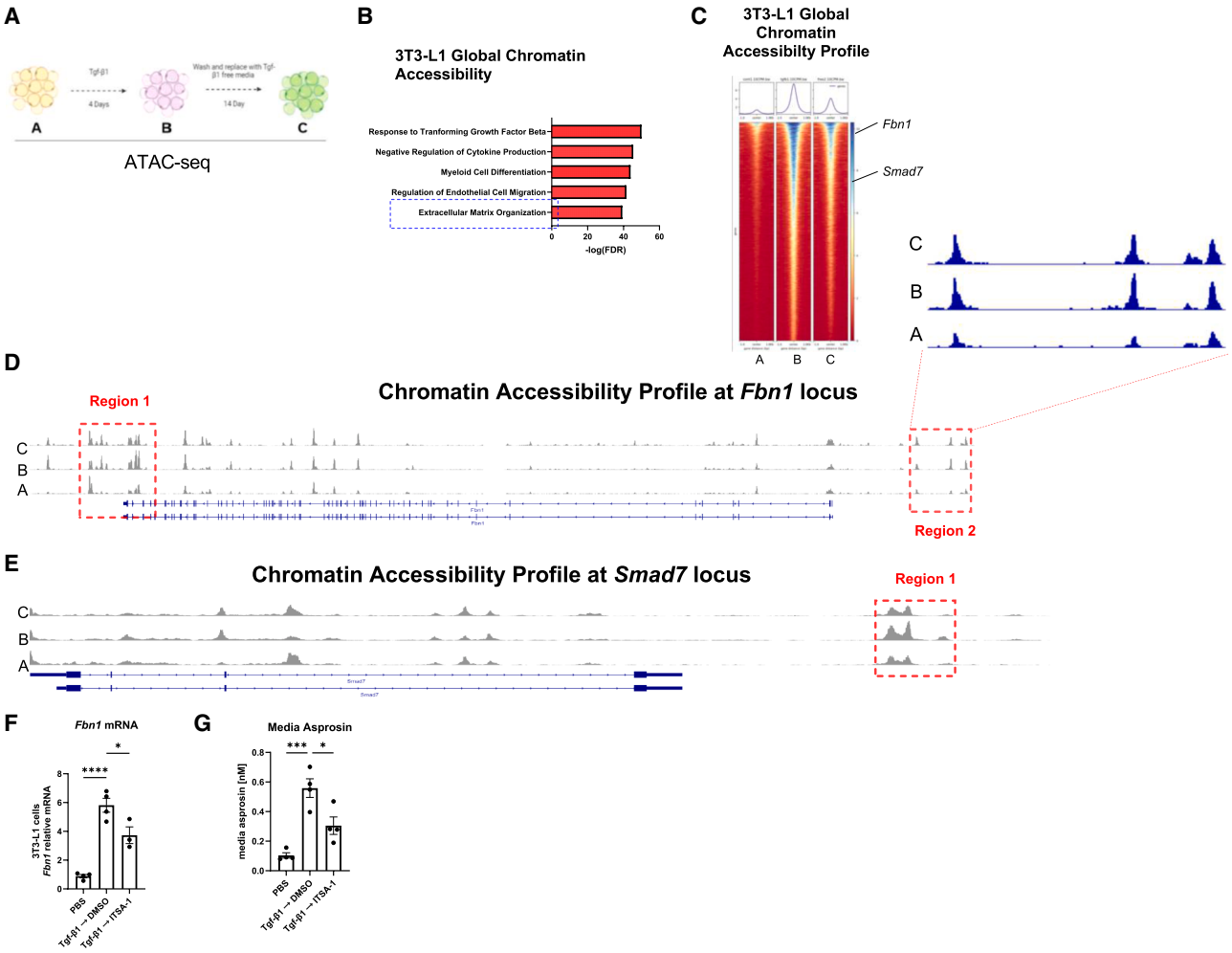

Figure 4. TGF-β1 alters chromatin accessibility to persistently upregulate *Fbn1* mRNA and plasma asprosin

(A) Experimental conditions for ATAC-seq matching those shown in Figure 3A.

(B) Gene Ontology (GO) pathway analysis of upregulated biological processes from ATAC-sequencing of samples exposed to TGF-β1 for 4 days (condition B vs. A).

(C) Heatmap generated from ATAC-seq data showing peaks considered significantly (4X) increased from diffBind analysis. Specifically, TGF-β1 broadly increases chromatin accessibility and many genes retain the increased accessibility even upon TGF-β1 withdrawal.

(D and E) Chromatin tracks at *Fbn1* and *Smad7* locus (respectively) from three separate conditions (control or untreated; TGF-β1 added for 4 days; and TGF-β1 added for 4 days followed by TGF-β1-free media incubation for 14 days). Red boxes highlight differential chromatin accessibility sites as found by diffBind algorithm analysis.

(F) qPCR showing relative mRNA levels of *Fbn1* in differentiated 3T3-L1 cells after incubation with PBS, or 4 days of TGF-β1 followed by 3 days of DMSO or ITSA-1 (100 μM) (n = 4 for PBS and TGF-β1→DMSO and n = 3 for TGF-β1→ITSA-1).

(G) Media asprosin detection with sandwich ELISA of differentiated 3T3-L1 cells after incubation with PBS, or 4 days of TGF-β1 followed by 3 days of DMSO or ITSA-1 (100 μM) (n = 4 for all groups).

Error bars represent mean ± SEM. *p < 0.05, **p < 0.01, ***p < 0.001, and ****p < 0.0001 by one-way ANOVA (F and G).

both food intake and body-weight regain (Figures S5H–S5K). This positive relationship between adiposity and circulating asprosin is consistent with observations in humans, where multiple studies have demonstrated that plasma asprosin is elevated in individuals with obesity and correlates positively with BMI, waist circumference, and body fat percentage.[18,38–40]

Because histone acetylation was required for TGF-β1-induced sustained *Fbn1* transcription and asprosin elevation, we next tested whether promoting histone deacetylation *in vivo* could blunt relapse. Treatment with the HDAC activator ITSA-1 prevented weight regain in mice with weight reduction compared with controls with vehicle treatment (Figures 5F and S5L). ITSA-1 had no effect on weight gain in mice without prior obesity fed HFD, excluding toxicity as a confounder (Figure S5M). ITSA-1 also reduced plasma asprosin levels (Figure 5G), linking its anti-relapse effect to suppression of asprosin production. Because Ptprd functions as the orexigenic receptor for asprosin, we next examined whether its activity is required for relapse.

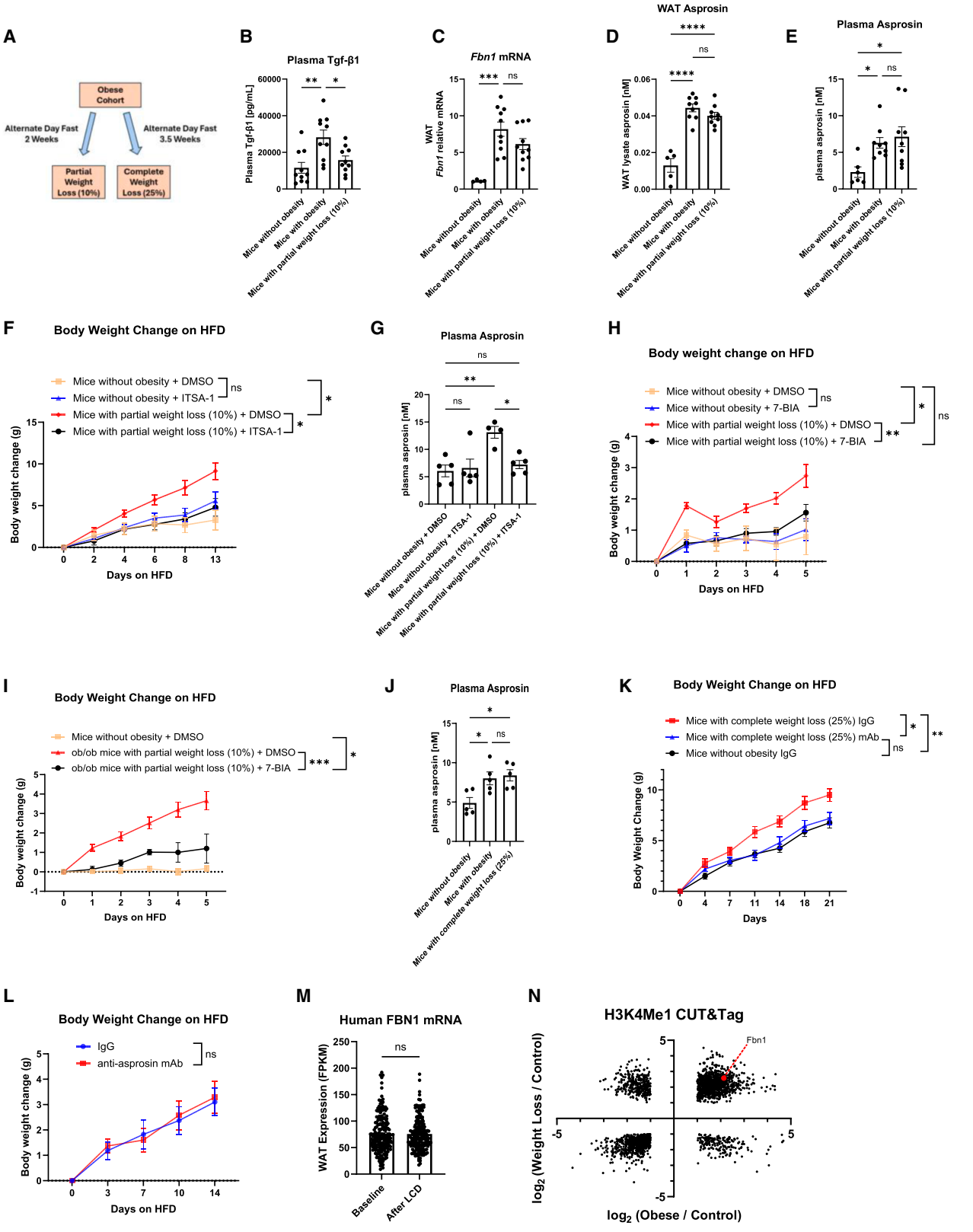

(legend on next page)

Administration of the Ptprd inhibitor 7-BIA[41] to mice with weight reduction significantly limited weight regain (Figures 5H and S5N), indicating that Ptprd signaling is necessary for obesity relapse. To validate this finding in a distinct model, we applied the same intervention to *ob/ob* mice subjected to alternate-day fasting that achieved 10% weight loss. Treatment with 7-BIA, in these *ob/ob* mice with weight-reduction significantly reduced weight regain (Figures 5I and S5O), confirming that asprosin-Ptprd signaling drives weight regain independently of leptin.

We next examined whether complete weight normalization affects this outcome. In a second DIO cohort, we implemented a 3.5-week fasting regimen that achieved an average 25% reduction in body weight, fully restoring the mice to the weight of age- and sex-matched controls without prior obesity (Figures 5A and S6A). Despite complete weight normalization, plasma asprosin levels remained elevated (Figure 5J). Upon HFD re-exposure, mice with prior obesity gained more weight than controls without prior obesity (Figures S6B and S6C). Neutralization of plasma asprosin with a monoclonal antibody completely prevented this excessive weight gain, aligning the mice with prior obesity with controls without prior obesity (Figures 5K and S6D). As previously shown,[42] the antibody had no effect in mice without prior obesity (Figures 5L and S6E), eliminating toxicity as a confounder.

Human data confirm what our mechanism predicts. If TGF-β1-induced chromatin modifications at the *FBN1* locus are self-sustaining and independent of ongoing cytokine signaling, then *FBN1* transcription and asprosin should remain elevated even after weight loss normalizes TGF-β1 levels. Indeed, in adipose tissue from subjects before and after a low-calorie diet, *FBN1* mRNA levels were unchanged despite 10% body-weight loss[43] (Figure 5M).

To explore the epigenetic basis for this persistence, we re-analyzed the adipose tissue dataset from Hinte et al.,[44] which profiled chromatin states in obese, post-weight-loss, and mice without prior obesity to generate an epigenomic atlas of adipose memory of prior obesity. Our analysis revealed that the H3K4Me1 peak associated with the *Fbn1* enhancer was elevated 4- to 8-fold in mice with obesity, and this increase was retained in mice post-weight-loss relative to controls without prior obesity (Figure 5N), indicating sustained enhancer activity in obesity and after weight loss. Gene Ontology analysis of persistently elevated peaks showed enrichment for "response to TGF-β," linking this cytokine pathway to long-term epigenetic activation of *Fbn1* (Figure S6F). Together, our reanalysis of the Hinte et al. dataset and our own ATAC-seq/CUT&Tag data support a model in which *Fbn1* and TGF-β-responsive enhancers contribute to adipose obesity memory.

Together, these findings identify a stable, TGF-β1-driven epigenetic program that sustains *Fbn1* transcription and plasma asprosin elevation after weight loss. This persistent hormonal state promotes hyperphagia and weight regain through Ptprd signaling, providing a unifying molecular explanation for the biological memory that drives obesity relapse across species.

Figure 5. Asprosin is necessary for obesity relapse

(A) Schematic of alternate-day fasting protocol used to generate partial weight loss (10%) or complete weight loss (25%) in mice. Briefly, DIO mice underwent an alternate-day fasting protocol using normal chow. Each cycle consisted of a 24-h fasting period followed by 24 h of *ad libitum* normal chow access. This was repeated for either 2 weeks to achieve partial weight loss (10%) or 3.5 weeks to achieve complete weight loss (25%).

(B) Mouse plasma sandwich ELISA for total TGF-β1 in 24-week-old male WT C57BL/6 mice, and 24-week-old male DIO mice before and after partial weight loss (10%). Plasma was collected before and after 2 weeks of alternate-day fasting (n = 10 for all groups).

(C) qPCR showing relative mRNA level of visceral adipose tissue *Fbn1* in 24-week-old male WT C57BL/6 mice, 24-week-old male DIO mice, and 26-week-old male mice with partial weight loss (10%) (n = 4 for WT group and n = 10 for other groups).

(D) Visceral adipose tissue lysate sandwich ELISA for asprosin in 24-week-old male WT C57BL/6 mice, 24-week-old male DIO mice, and 26-week-old male mice with partial weight loss (10%) (n = 5 for WT group and n = 9 for other groups).

(E) Mouse plasma sandwich ELISA for asprosin of 24-week-old-male WT C57BL/6 mice, 24-week-old-male DIO mice, and 26-week-old-male mice with partial weight loss (10%) (n = 6 for WT group and n = 9 for other groups).

(F and G) Body weight change and mouse plasma sandwich ELISA for asprosin (respectively) in 28-week-old male mice with partial weight loss (10%) and age-matched controls without obesity i.p. treated with DMSO or ITSA-1 (4 mg/kg) daily for 5 days, and subsequently provided *ad libitum* HFD over 13 days. Plasma was collected at the end of 13 days on HFD (n = 4 for partial weight loss [10%] + DMSO and n = 5 for all other groups).

(H) Body weight change of 27-week-old mice with partial weight loss (10%) and age-matched controls without prior obesity on *ad libitum* HFD while receiving daily i.p. injections of DMSO or 7-BIA (150 μg) (n = 5 for all groups).

(I) Body weight change of 12-week-old *ob/ob* mice subjected to partial weight loss (10%) with alternate-day fasting and recombinant leptin injection (10 μg) on feeding days. *Ob/ob* mice and age-matched controls without prior obesity were on *ad libitum* HFD while receiving daily i.p. injections of DMSO or 7-BIA (300 μg) (n = 10 for lean + DMSO, n = 7 for *ob/ob* mice with partial weight loss [10%] + DMSO, and n = 8 for *ob/ob* mice with partial weight loss [10%] + 7-BIA). We did not include a never-obese + 7-BIA group as we have previously shown that there is no difference in body weight change compared with never-obese + DMSO group (Figure 5H).

(J) Mouse plasma sandwich ELISA for asprosin on 28-week-old male WT C57BL/6 mice, 24-week-old male DIO mice, and 28-week-old male mice with complete weight loss (25%) (n = 5 per group).

(K) Body weight change of 28-week-old male WT C57BL/6 mice without prior obesity, 28-week-old male mice with complete weight loss (25%) on *ad libitum* HFD while receiving daily i.p. injections of IgG or anti-asprosin monoclonal antibody (5.55 μg/g mouse) (n = 10 for lean IgG group and n = 6 for all other groups).

(L) Body weight change of 12-week-old-male WT C57BL/6 mice on *ad libitum* HFD while receiving daily i.p. injections of IgG or anti-asprosin monoclonal antibody (5.55 μg/g mouse) (n = 7 for IgG and n = 10 for anti-asprosin mAb).

(M) FPKM expression data of *FBN1* from RNA sequencing analysis of a mined public dataset examining expression at baseline and after a low-calorie diet.

(N) Scatterplot generated from analyzing publicly available data showing $\log_2$ fold changes in H3K4Me1 CUT&Tag signal for obese vs. control (x axis) and weight loss vs. control (y axis). Each point represents a genomic region; the red point marks the *Fbn1* locus with increased enrichment in both conditions.

Error bars represent mean ± SEM. $^{*}p < 0.05$, $^{**}p < 0.01$, $^{***}p < 0.001$, and $^{****}p < 0.0001$ by one-way ANOVA (B–E, G, and J), two-way ANOVA (F, H, I, K, and L), and unpaired two-sided t test (M).

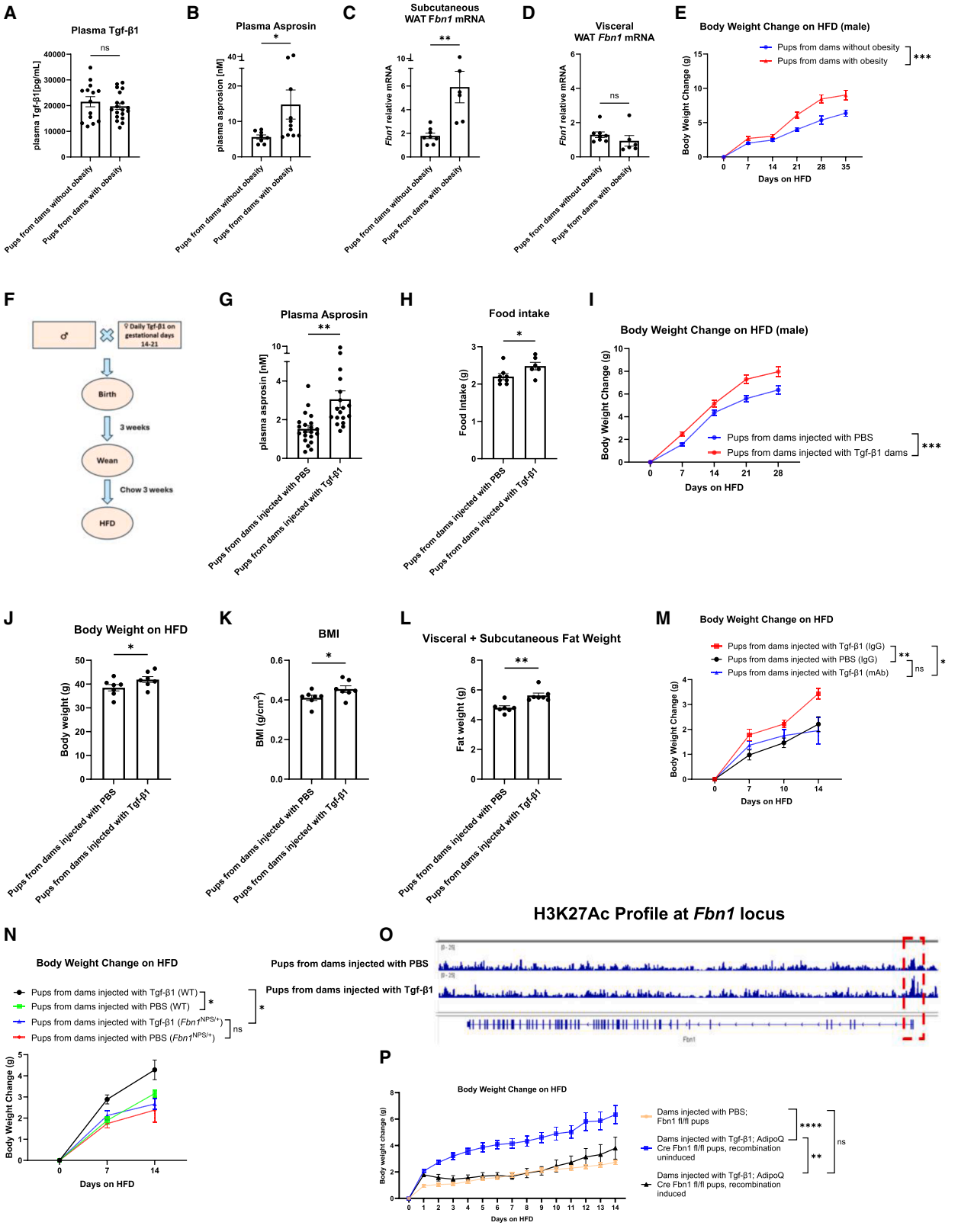

(legend on next page)

Maternal TGF-β1-induced *Fbn1* activation in fetal adipose tissue drives obesity inheritance

Childhood obesity arises from intertwined environmental, societal, and biological influences.[45] While environmental and behavioral factors are modifiable, the biological mechanisms transmitting obesity risk across generations remain poorly defined.[45–49] Maternal or pre-pregnancy BMI is among the strongest predictors of obesity in children,[4–7,11,12] yet the molecular basis of this association is unknown.

Because TGF-β1 crosses the placenta,[50] we hypothesized that elevated maternal TGF-β1 in obesity programs the offspring to chronically upregulate *Fbn1* and overproduce asprosin. DIO females were mated with males without prior obesity, and their pups were placed on normal chow after weaning. Although plasma TGF-β1 levels were comparable between groups, pups from dams with obesity displayed higher plasma asprosin and increased *Fbn1* expression confined to subcutaneous WAT (Figures 6A–6D). This depot specificity aligns with developmental timing, as subcutaneous fat forms prenatally while visceral fat develops postnatally,[51] indicating selective *in utero* priming by maternal TGF-β1.

Despite similar body weights on chow, male and female pups from dams with obesity gained substantially more weight when exposed to an HFD, demonstrating a programmed susceptibility to obesity and eliminating sexual dimorphism as a consideration (Figures 6E and S7A–S7E).

To test whether maternal TGF-β1 is sufficient to induce this phenotype, we administered recombinant TGF-β1 to females without obesity during late gestation. Their offspring exhibited elevated plasma asprosin, increased food intake, and exaggerated weight gain on HFD, recapitulating the effects of obesity in mothers (Figures 6F–6I and S8A–S8E). Extended HFD exposure revealed faster weight gain, higher body mass index, and greater adiposity without changes in linear growth (Figures 6J–L and S8F–S8H), confirming accelerated obesity development.

Neutralizing asprosin pharmacologically completely prevented weight gain in offspring of dams with TGF-β1-treatment (Figures 6M and S8I), and constitutive reduction of asprosin in *Fbn1*$^{NPS/+}$ offspring produced the same outcome (Figures 6N and S8J), further supporting the requirement for asprosin in this process. To determine whether maternal asprosin itself drives inheritance, we elevated plasma asprosin in females

Figure 6. Asprosin is necessary for obesity inheritance

(A) Mouse plasma sandwich ELISA for total TGF-β1 in 3-week-old male pups generated from mating obese or WT C57BL/6 dams without obesity with WT C57BL/6 males without obesity (n = 14 for pups from dams without obesity and n = 19 for pups from dams with obesity).

(B) Mouse plasma sandwich ELISA for asprosin in 3-week-old male pups generated from mating obese or WT C57BL/6 dams without obesity with WT C57BL/6 males without obesity (n = 8 for pups from dams without obesity and n = 11 for pups from dams with obesity).

(C and D) qPCR showing relative mRNA level of subcutaneous and visceral (respectively) adipose tissue *Fbn1* 4 weeks after weaning in male pups generated from mating obese or WT C57BL/6 dams without obesity with WT C57BL/6 males without obesity (n = 8 for pups from dams without obesity and n = 6 for pups from dams with obesity).

(E) Body weight change of male pups on *ad libitum* HFD generated from mating obese or WT C57BL/6 dams without obesity with WT C57BL/6 males without obesity. Pups were weaned and put on normal chow, then given HFD on day 33 after weaning (n = 14 for pups from dams without obesity and n = 8 for pups from dams with obesity).

(F) Schematic showing breeding protocol of maternal TGF-β1 treatment during gestational days 14–21 and timeline for offspring analyses.

(G) Mouse plasma sandwich ELISA for asprosin in male pups generated from TGF-β1 or PBS-injected FVB/NJ dams without obesity mated with WT C57BL/6 males without obesity (n = 21 for pups from dams injected with PBS and n = 18 for pups from dams injected with TGF-β1).

(H) 24 h food intake of male pups generated from TGF-β1 or PBS-injected FVB/NJ dams without obesity, mated with WT C57BL/6 males without obesity, 2 weeks after weaning, and on *ad libitum* dustless diet (n = 8 for pups from dams injected with PBS and n = 6 for pups from dams injected with TGF-β1).

(I) Body weight change of male pups on *ad libitum* HFD generated from TGF-β1 or PBS-injected FVB/NJ dams without obesity mated with WT C57BL/6 males without obesity. Pups were weaned and put on normal chow then given HFD on day 20 after weaning (n = 22 for pups from dams injected with PBS and n = 18 for pups from dams injected with TGF-β1).

(J–L) Body weight, BMI, and visceral + subcutaneous fat depot weight (respectively) of male pups on *ad libitum* HFD for 52 days generated from TGF-β1 or PBS-injected FVB/NJ dams without obesity mated with WT C57BL/6 males without obesity. The pups were put on HFD 6 weeks after weaning (n = 7 for all groups).

(M) Body weight change on *ad libitum* HFD of female pups generated from TGF-β1 or PBS-injected FVB/NJ dams without obesity mated with WT C57BL/6 males without obesity. Pups were weaned and put on normal chow, then given HFD on day 14 after weaning. Pups were given daily injections of IgG or anti-asprosin monoclonal antibody (5.55 μg/g mouse) (n = 8 for pups from dams injected with PBS [IgG], n = 5 for pups from dams injected with TGF-β1 [IgG], and n = 6 for pups from dams injected with TGF-β1 [mAb]). We did not include pups from dams injected with PBS (mAb) group because we have previously shown that mAb treatment does not affect body weight in lean mice when compared with IgG (Figure S6E).

(N) Body weight change of offspring from dams treated with PBS and TGF-β1 during late gestation. Pregnant dams that had been mated with male *Fbn1*$^{NPS/+}$ mice without obesity received twice daily injections of PBS or TGF-β1 from gestational days 14–21. The resulting litters contained both WT and *Fbn1*$^{NPS/+}$ offspring, which were weaned onto a chow diet, then switched to *ad libitum* HFD 18 days post-weaning. Body weight was recorded over the subsequent 14 days on HFD (n = 13 for pups from dams injected with TGF-β1 [WT], n = 8 for pups from dams injected with PBS [WT], n = 9 for pups from dams injected with TGF-β1 [*Fbn1*$^{NPS/+}$], and n = 5 for pups from dams injected with PBS [*Fbn1*$^{NPS/+}$]).

(O) Schematic showing H3K27ac profile at *Fbn1* locus from CUT&Tag sequencing of subcutaneous adipose tissue of 15-week-old pups born from dams injected with PBS or TGF-β1. Red box highlights significant peak difference where H3K27ac occupancy was increased by 65% in the pups from dams injected with TGF-β1 relative to pups from dams injected with PBS. This corresponds to the *Fbn1* promoter.

(P) Pregnant dams received PBS or TGF-β1 on gestational days 14–21. Offspring were weaned to chow for 1 week, then given tamoxifen (100 mg/kg i.p., 5 days) or vehicle to induce adipose-specific *Fbn1* deletion in *Adipoq-Cre; Fbn1* exon 66$^{flx/flx}$ pups. After 3 weeks, all pups, including PBS-exposed *Adipoq-Cre* (−); *Fbn1* exon 66$^{flx/flx}$ controls were switched to a high-fat diet at the same age, and body-weight change was recorded daily for 14 days (n = 12 for PBS→*Adipoq-Cre* (−) *Fbn1* exon 66$^{flx/flx}$ controls and n = 6 for all other groups). We did not include the 4th group of PBS-injected dams, *Fbn1*$^{fl/fl}$ subsequently injected with tamoxifen, as we have previously shown that tamoxifen injection in lean mice with appropriate washout does not affect body weight (Figures S10F and S10G).

Error bars represent mean ± SEM. *p < 0.05, **p < 0.01, ***p < 0.001, and ****p < 0.0001 by unpaired two-sided t test (A, C, D, G, H, K, and L), unpaired one-sided t test (B and J), and two-way ANOVA (E, I, M, N, and P).

without obesity using AAV8-asprosin. Offspring from dams treated with AAV8-asprosin showed normal asprosin levels and body weight on both chow and HFD, excluding maternal asprosin as the causal factor (Figures S9A–S9E).

To probe the molecular mechanism, we performed CUT&Tag for H3K27ac in subcutaneous adipose tissue from 15-week-old pups of dams treated with TGF-β1 or PBS. Offspring of dams treated with TGF-β1 showed a 65% increase in H3K27ac enrichment at the *Fbn1* promoter, consistent with sustained enhancer activation, while *Smad7* remained unchanged (Figures 6O and S10A).

Finally, to directly test the requirement of adipose-derived asprosin for this phenotype in adulthood, independent of developmental effects, we used a mouse with an inducible, adipocyte-specific *Fbn1* knockout (Adipoq-CreERT2; *Fbn1*$^{fl/fl}$) gene. In adults, induction produced selective recombination in adipose tissue and lowered plasma asprosin (Figures S10B–S10E). For 13 weeks following induction, knockout and control littermates maintained on chow exhibited indistinguishable body-weight trajectories, indicating that the induction procedure itself had no metabolic effect (Figures S10F and S10G). Upon transition to an HFD, however, knockout mice displayed a marked resistance to weight gain and demonstrated reduced food intake (Figures S10F–S10H), consistent with loss of adipose-derived asprosin and in agreement with findings from Lu et al.,[52] who used a constitutive adipose-specific deletion rather than the inducible model employed here. When the same inducible deletion was triggered post-weaning in offspring of dams treated with TGF-β1, it completely prevented the accelerated weight gain observed in their uninduced littermates, restoring normal body-weight trajectories equivalent to offspring of dams treated with PBS (Figures 6P and S10I).

Together, these findings demonstrate that maternal TGF-β1, rather than maternal asprosin, crosses the placenta to epigenetically activate *Fbn1* transcription in fetal adipose tissue. This persistent activation sustains elevated plasma asprosin, predisposing offspring to obesity when challenged with an obesogenic environment. Convergent evidence from pharmacologic neutralization, constitutive genetic reduction, and inducible adipocyte-specific deletion supports a hormone-driven, epigenetically encoded mechanism for the intergenerational transmission of obesity susceptibility.

DISCUSSION

This study identifies a cytokine-driven transcriptional mechanism that contributes to two long-standing features of obesity: the universal tendency toward relapse after weight loss and the increased susceptibility of offspring born to mothers with obesity (Figure 7). This mechanism converts an inflammatory signal into durable hormone overproduction, providing a molecular explanation for obesity's persistence and intergenerational transmission. The obesity-associated elevation of TGF-β1 initiates stable *Fbn1* transcription in adipocytes through canonical receptor and Smad4 signaling coupled to p300/CBP-dependent chromatin remodeling. This results in sustained asprosin production long after TGF-β1 levels normalize, suggesting that adipose tissue can retain a transcriptional memory of prior obesity. The persistent elevation of asprosin establishes a lasting orexigenic drive that favors weight regain even after complete metabolic recovery.

Asprosin biology is well established across genetic, biochemical, pharmacological, and physiological experimental platforms. Loss-of-function mutations in *FBN1* and corresponding mouse models revealed markedly reduced circulating asprosin accompanied by profound leanness, reduced appetite, and suppressed hepatic glucose production across species[13,16]—establishing the initial causal link between the hormone and systemic metabolic regulation. Independent laboratories subsequently showed that plasma asprosin rises during fasting and in obesity,[53,54] and that recombinant protein drives hepatic cAMP production and glucose output across multiple orthogonal systems.[52,55–58] Adipose-targeted deletion of *Fbn1* lowered circulating asprosin and protected against diet-induced weight gain and hyperglycemia,[52] identifying WAT as the dominant metabolic source of the hormone. These relationships are corroborated across multiple independent human studies in which plasma asprosin correlates positively with adiposity.[18,38–40] Beyond its glucogenic actions, asprosin promotes feeding through PTPRD-dependent activation of AgRP neurons,[13,15,42,59] an orexigenic pathway independently validated.[14] Receptor-level studies have further refined mechanistic coherence: a recent study independently replicated both the glucogenic and orexigenic functions of asprosin across species, confirmed PTPRD as the orexigenic receptor through zebrafish CRISPR knockout, and identified PTPRF as the cognate hepatic glucogenic receptor—supporting a conserved receptor family in which paralogs mediate asprosin's central and peripheral actions through non-overlapping mechanisms.[60] Additional evolutionary evidence came from identification of a C-terminal fibrillin-2 (*FBN2*) fragment with glucogenic and orexigenic activity in non-mammalian vertebrates,[61] indicating deep conservation of the fibrillin-derived hormone axis. Together, these convergent findings across species, receptor systems, and experimental modalities establish asprosin as a reproducible and causally active regulator of energy balance, providing the biological foundation upon which the upstream epigenetic mechanism described here operates.

The evidence for the TGF-β1 to *Fbn1* to asprosin pathway is multilayered. At the transcriptional level, TGF-β1 increases RNA polymerase II recruitment at the *Fbn1* locus and requires intact Tgfbr2 and Smad4 signaling. At the chromatin level, ATAC-seq and CUT&Tag analyses reveal lasting accessibility and H3K27 acetylation at *Fbn1* regulatory regions. At the physiological level, interventions at distinct nodes of the pathway such as histone deacetylation, hormone neutralization, and receptor inhibition each prevent weight regain. The concordant outcomes across these independent manipulations show that *Fbn1* acetylation, asprosin, and Ptprd signaling together constitute a necessary pathway for relapse.

The neuroendocrine adaptations of the weight-reduced state have been previously established. Following weight loss, circulating leptin and peptide YY decline while ghrelin rises, collectively shifting hypothalamic circuits toward increased appetite and reduced satiety.[62] Concurrently, skeletal muscle contractile efficiency increases, sympathetic tone decreases, and resting

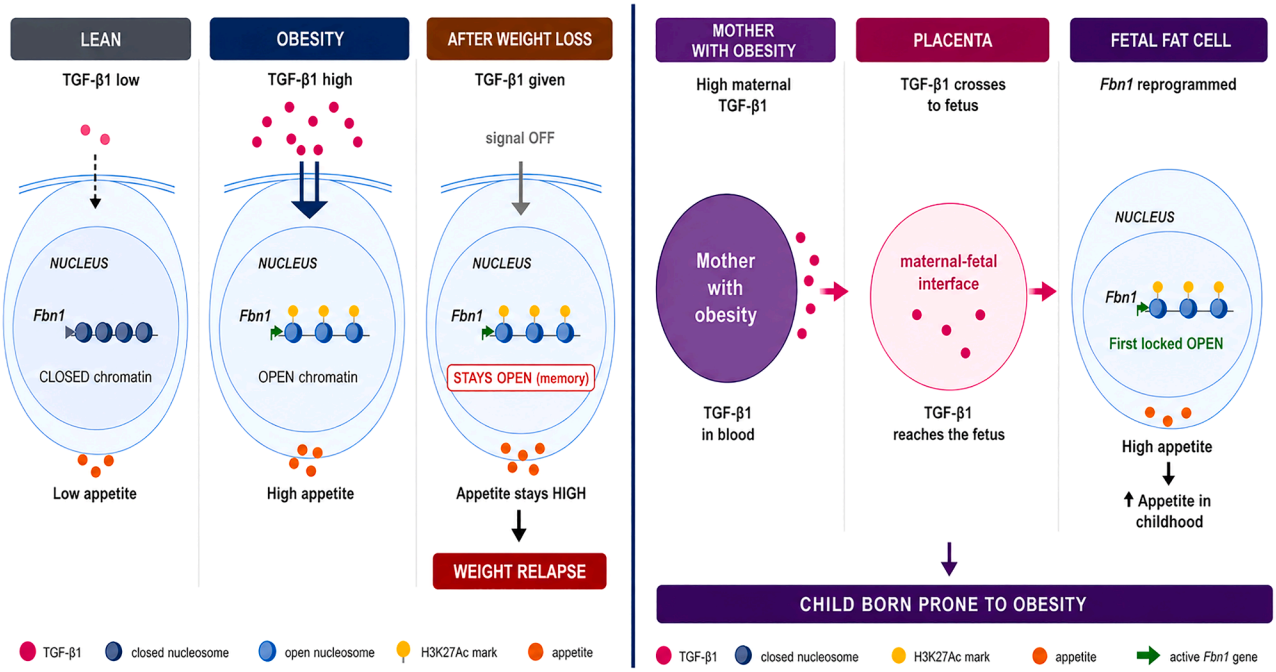

Figure 7. Mechanism of obesity relapse and inheritance

(Left) Schematic showing how TGF-β1 drives chromatin remodeling at the *FBN1* locus to establish a durable, weight-relapse-promoting epigenetic state. In the state without obesity, low TGF-β1 maintains *FBN1* chromatin in a condensed, transcriptionally silent conformation, corresponding to low asprosin output. With obesity, elevated TGF-β1 signaling opens *FBN1* chromatin, marked by deposition of H3K27ac, driving increased *FBN1* transcription and asprosin secretion. After weight loss, although TGF-β1 signaling is withdrawn, the open chromatin conformation at *FBN1* is retained as an epigenetic memory, sustaining elevated asprosin output and appetite, and thereby promoting weight relapse.

(Right) Schematic showing how maternal TGF-β1 crosses the placental barrier and enters fetal adipose tissue, where it remodels chromatin at the *FBN1* locus from a condensed, silenced state to an open, accessible conformation. This epigenetic reprogramming increases *FBN1* transcription and asprosin secretion. Because these chromatin changes persist beyond TGF-β1 withdrawal, asprosin output remains constitutively elevated, establishing a durable epigenetic basis for obesity susceptibility in offspring.

energy expenditure falls: all adaptations that create pressure toward weight regain.[63,64] However, the precise molecular driver that renders the relapse state durable and transmissible has not been identified. Our contributions add to this framework by identifying a specific peripheral driver that maintains a relapse-prone state. Weight-loss interventions such as alternate-day fasting or GLP-1 receptor agonists reduce body weight during active treatment but are universally followed by regain once therapy ends.[36] The data here suggest that this failure of maintenance reflects an underlying transcriptional state within adipose tissue that continues to drive asprosin production even after weight normalization. Interventions that reset or suppress the *FBN1*-to-asprosin-to-PTPRD axis may enable durable weight-loss maintenance by eliminating the endocrine memory of prior obesity.

This same mechanism is consistent with the intergenerational transmission of obesity risk. Maternal TGF-β1 crosses the placenta and establishes a persistent acetylated chromatin state at the *Fbn1* promoter in fetal adipose tissue, driving elevated plasma asprosin and heightened susceptibility to weight gain later in life. This predisposition depends entirely on asprosin because antibody neutralization, constitutive genetic depletion, or inducible adipocyte-specific *Fbn1* deletion in offspring each prevent the phenotype. These findings identify a defined molecular event that links maternal metabolic status to offspring adipose programming, providing a mechanistic explanation for one of the strongest and most consistent predictors of childhood obesity.

TGF-β1 is not unique to obesity but rises in diverse physiological and pathological states, including acute infection,[65,66] sterile tissue injury such as fracture healing,[67] and normal pregnancy.[68] Interestingly, epidemiologic observations suggest that viral infections such as adenovirus-36 increase adiposity across species and are associated with elevated body weight in seropositive humans.[69–71] Maternal infection during pregnancy correlates with increased obesity risk in offspring,[72] and repeated childhood infections predict higher BMI in adolescence, consistent with durable metabolic effects of early immune activation.[73] However, our causal claims are restricted to chronic, obesity-level TGF-β1 elevations, which we demonstrate as sufficient to establish a durable epigenetic state at the *Fbn1* locus that persists independent of the original stimulus. Whether the shorter-lived TGF-β1 pulses that occur during normal pregnancy, infections, or tissue repair are sufficient to produce the same chromatin outcome remains an open and important question. The epidemiological observations that viral infections and maternal illness correlate with elevated body weight and increased offspring obesity risk are intriguing in light of our mechanism, but at present these associations should be interpreted as hypotheses warranting future mechanistic and longitudinal investigation.

More broadly, the findings support a model in which adipose tissue can convert transient inflammatory signals into long-lasting transcriptional programs. Cytokine-induced chromatin remodeling may represent a general mechanism by which episodic immune stimuli shape future metabolic state, analogous to trained immunity in myeloid cells or experience-dependent plasticity in the nervous system. Systematic discovery of such endocrine memory mechanisms will clarify how temporary perturbations become chronic physiological states and may reveal opportunities for therapeutic reversal. In this view, obesity recurrence and intergenerational transmission may be active consequences of a stable transcriptional state established by prior inflammatory input. Understanding and ultimately erasing this molecular memory will be essential for efforts to break the self-sustaining cycle of obesity.

Limitations of the study

This work is primarily based on experimental mouse models and *in vitro* systems and therefore cannot establish the full causal contribution of the TGF-β1-*Fbn1*-asprosin axis to obesity relapse or inheritance in humans. Human data in this study and in the literature are observational and limited in size and temporal resolution, so the extent to which the adipose "memory" mechanism identified here operates in human obesity remains to be defined. Inheritance experiments rely on gestational exposure paradigms that reproduce obesity-level TGF-β1 elevations but do not capture the full complexity of human maternal obesity or its many correlates. Epigenetic interventions such as ITSA-1 treatment are not specific to *Fbn1* and may affect other loci and pathways. Within the confines of the mouse models studied here, the TGF-β1-*Fbn1*-asprosin-Ptprd pathway is necessary for relapse and inheritance, but it is likely to act in the context of additional organism-level adaptations described previously (e.g., changes in leptin, ghrelin, gut hormones, autonomic tone, and energy expenditure) that were not directly tested in this work.

RESOURCE AVAILABILITY

Lead contact

Requests for further information and resources should be directed to and will be fulfilled by the lead contact, Atul R. Chopra (atul.chopra@case.edu).

Materials availability

All data used in the analysis is available to any researcher for purposes of reproducing or extending the analysis in source data files. Further information and requests for resources and reagents should be directed to and will be fulfilled by the corresponding author.

Data and code availability

- All data reported in this paper will be shared by the lead contact upon request. All raw and analyzed sequencing data generated in this study have been deposited in GEO (GSE277913 and GSE277916).
- This paper does not report original code.
- Any additional information required to reanalyze the data reported in this paper is available from the lead contact upon request.

ACKNOWLEDGMENTS

The use of the Yale Center for Genome Analysis is acknowledged for ATAC sequencing. The use of the Genomics Core Facility of the CWRU School of Medicine's Genetics and Genome Sciences Department is acknowledged for RNA sequencing. We thank members of the Chopra lab for helpful suggestions and critical reading of the manuscript. A.R.C. is supported by the NIDDK (R01DK118290 and R01DK1025295403) and the Harrington Investigatorship. B.C.K., Y.F.C., and B.B. were supported in part by the NIH grant T32 GM007250. Y.F.C. was additionally supported by the NIH grant T32 GM135081 and by the Harrington Discovery Institute. I.M. was supported by the NIH grant P20GM156679 and the Diabetes Action Research and Education Foundation.

AUTHOR CONTRIBUTIONS

B.C.K. and A.R.C. conceived the project, experimental design and writing/editing of the manuscript. A.R.C. was responsible for funding acquisition to enable the project. B.C.K. and C.K. performed the majority of procedures, data acquisition, and analyses. Y.F.C. assisted with RNA sequencing and ATAC sequencing planning and data analysis. K.S., N.A., and S.F. replicated key *in vitro* and *in vivo* data independently. A.L., H.O., B.B., E.S.S., J.M., and I.M. assisted with data acquisition and data discussion.

DECLARATION OF INTERESTS

A.R.C. has been awarded asprosin-related patents. A.R.C. is a co-founder, equity holder, and previously an officer of Aceragen; a co-inventor on related intellectual property; and a co-founder, equity holder, and officer of Recall Therapeutics and Pathway21. B.B. is an equity holder and officer of Recall Therapeutics.

DECLARATION OF GENERATIVE AI AND AI-ASSISTED TECHNOLOGIES IN THE WRITING PROCESS

During the preparation of this work, GPT-4o, GPT-5, and Claude Opus 5 were used for language refinement and to assist in creating the initial versions of the Figure 7 conceptual schematic and the graphical abstract. These materials were developed under extensive author direction and were subsequently edited and reviewed by the authors to ensure scientific accuracy. The authors carefully reviewed and edited all AI-assisted content as necessary and take full responsibility for the content and accuracy of the publication.

STAR★METHODS

Detailed methods are provided in the online version of this paper and include the following:

- KEY RESOURCES TABLE
- EXPERIMENTAL MODEL AND STUDY PARTICIPANT DETAILS
  - Mice
  - Inducible, adipocyte-specific *Fbn1* knockout mouse line
  - Cell lines and reagents
- METHOD DETAILS
  - Alternate day fasting
  - In-vivo cytokine treatment
  - Pharmacologic interventions and inhibitor treatments
  - TGF-β1 injection into FVB/NJ females
  - Metabolic caging and food intake assessment
  - Differentiation of 3T3-L1 cells
  - shRNA knockdown
  - Quantitative PCR
  - mRNA half-life
  - Asprosin ELISA
  - Adeno-associated virus injection
  - RNA sequencing
  - ATAC sequencing
  - CUT&Tag sample preparation
  - Peak calling and analysis
  - Diffbind analysis
  - *In vivo* anti-asprosin mAb treatment

- Third party independent validation
- QUANTIFICATION AND STATISTICAL ANALYSIS

SUPPLEMENTAL INFORMATION

Supplemental information can be found online at https://doi.org/10.1016/j.celrep.2026.117809.

Received: October 24, 2024
Revised: May 4, 2026
Accepted: July 22, 2026
Published: August 11, 2026

REFERENCES

1. Phelps, N.H., Singleton, R.K., Zhou, B., Heap, R.A., Mishra, A., Bennett, J.E., Paciorek, C.J., Lhoste, V.P., Carrillo-Larco, R.M., Stevens, G.A., et al. (2024). Worldwide trends in underweight and obesity from 1990 to 2022: a pooled analysis of 3663 population-representative studies with 222 million children, adolescents, and adults. Lancet *403*, 1027–1050. https://doi.org/10.1016/s0140-6736(23)02750-2.
2. Wing, R.R., and Phelan, S. (2005). Long-term weight loss maintenance. Am. J. Clin. Nutr. *82*, 222S–225S. https://doi.org/10.1093/ajcn.82.1.222s.
3. Kaplan, L.M., Golden, A., Jinnett, K., Kolotkin, R.L., Kyle, T.K., Look, M., Nadglowski, J., O'Neil, P.M., Parry, T., Tomaszewski, K.J., et al. (2018). Perceptions of Barriers to Effective Obesity Care: Results from the National ACTION Study. Obesity *26*, 61–69. https://doi.org/10.1002/oby.22054.
4. Heslehurst, N., Vieira, R., Akhter, Z., Bailey, H., Slack, E., Ngongalah, L., Pemu, A., and Rankin, J. (2019). The association between maternal body mass index and child obesity: A systematic review and meta-analysis. PLoS Med. *16*, e1002817. https://doi.org/10.1371/journal.pmed.1002817.
5. Voerman, E., Santos, S., Patro Golab, B., Amiano, P., Ballester, F., Barros, H., Bergström, A., Charles, M.-A., Chatzi, L., Chevrier, C., et al. (2019). Maternal body mass index, gestational weight gain, and the risk of overweight and obesity across childhood: An individual participant data meta-analysis. PLoS Med. *16*, e1002744. https://doi.org/10.1371/journal.pmed.1002744.
6. Gaillard, R., Santos, S., Duijts, L., and Felix, J.F. (2016). Childhood Health Consequences of Maternal Obesity during Pregnancy: A Narrative Review. Ann. Nutr. Metab. *69*, 171–180. https://doi.org/10.1159/000453077.
7. Hsu, P.-C., Hwang, F.-M., Chien, M.-I., Mui, W.-C., and Lai, J.-M. (2022). The impact of maternal influences on childhood obesity. Sci. Rep. *12*, 6258. https://doi.org/10.1038/s41598-022-10216-w.
8. McPherson, R. (2007). Genetic contributors to obesity. Can. J. Cardiol. *23*, 23A–27A. https://doi.org/10.1016/s0828-282x(07)71002-4.
9. Silventoinen, K., Jelenkovic, A., Sund, R., Hur, Y.-M., Yokoyama, Y., Honda, C., Hjelmborg, J.v., Möller, S., Ooki, S., Aaltonen, S., et al. (2016). Genetic and environmental effects on body mass index from infancy to the onset of adulthood: an individual-based pooled analysis of 45 twin cohorts participating in the COllaborative project of Development of Anthropometrical measures in Twins (CODATwins) study 1–3. Am. J. Clin. Nutr. *104*, 371–379. https://doi.org/10.3945/ajcn.116.130252.
10. Albuquerque, D., Nóbrega, C., Manco, L., and Padez, C. (2017). The contribution of genetics and environment to obesity. Br. Med. Bull. *123*, 159–173. https://doi.org/10.1093/bmb/ldx022.
11. Barroso, C.S., Roncancio, A., Hinojosa, M.B., and Reifsnider, E. (2012). The Association between Early Childhood Overweight and Maternal Factors. Child. Obes *8*, 449–454. https://doi.org/10.1089/chi.2011.0094.
12. Janjua, N.Z., Mahmood, B., Islam, M.A., and Goldenberg, R.L. (2012). Maternal and Early Childhood Risk Factors for Overweight and Obesity among Low-Income Predominantly Black Children at Age Five Years: A Prospective Cohort Study. J. Obes. *2012*, 457173. https://doi.org/10.1155/2012/457173.
13. Duerrschmid, C., He, Y., Wang, C., Li, C., Bournat, J.C., Romere, C., Saha, P.K., Lee, M.E., Phillips, K.J., Jain, M., et al. (2017). Asprosin is a centrally-acting orexigenic hormone. Nat. Med. *23*, 1444–1453. https://doi.org/10.1038/nm.4432.
14. Feng, B., Liu, H., Mishra, I., Duerrschmid, C., Gao, P., Xu, P., Wang, C., and He, Y. (2023). Asprosin promotes feeding through SK channel–dependent activation of AgRP neurons. Sci. Adv. *9*, eabq6718. https://doi.org/10.1126/sciadv.abq6718.
15. Mishra, I., Xie, W.R., Bournat, J.C., He, Y., Wang, C., Silva, E.S., Liu, H., Ku, Z., Chen, Y., Erokwu, B.O., et al. (2022). Protein tyrosine phosphatase receptor δ serves as the orexigenic asprosin receptor. Cell Metab. *34*, 549–563.e8. https://doi.org/10.1016/j.cmet.2022.02.012.
16. Romere, C., Duerrschmid, C., Bournat, J., Constable, P., Jain, M., Xia, F., Saha, P.K., Del Solar, M., Zhu, B., York, B., et al. (2016). Asprosin, a Fasting-Induced Glucogenic Protein Hormone. Cell *165*, 566–579. https://doi.org/10.1016/j.cell.2016.02.063.
17. Basu, B., Jain, M., and Chopra, A.R. (2021). Caudamins, a new subclass of protein hormones. Trends Endocrinol. Metab. *32*, 1007–1014. https://doi.org/10.1016/j.tem.2021.09.005.
18. Lv, D., Wang, Z., Meng, C., Li, Y., and Ji, S. (2024). A study of the relationship between serum asprosin levels and MAFLD in a population undergoing physical examination. Sci. Rep. *14*, 11170. https://doi.org/10.1038/s41598-024-62124-w.
19. Mahat, R.K., Jantikar, A.M., Rathore, V., and Panda, S. (2024). Circulating asprosin levels in type 2 diabetes mellitus: A systematic review and meta-analysis. Clin. Epidemiol. Glob. Health *25*, 101502. https://doi.org/10.1016/j.cegh.2023.101502.
20. Moradi, N., Fouani, F.Z., Vatannejad, A., Bakhti Arani, A., Shahrzad, S., and Fadaei, R. (2021). Serum levels of Asprosin in patients diagnosed with coronary artery disease (CAD): a case-control study. Lipids Heal. Dis. *20*, 88. https://doi.org/10.1186/s12944-021-01514-9.
21. Mirr, M., Braszak-Cymerman, A., Ludziejewska, A., Kręgielska-Narożna, M., Bogdański, P., Bryl, W., and Owecki, M. (2023). Serum Asprosin Correlates with Indirect Insulin Resistance Indices. Biomedicines *11*, 1568. https://doi.org/10.3390/biomedicines11061568.
22. Lin, Y., Nakachi, K., Ito, Y., Kikuchi, S., Tamakoshi, A., Yagyu, K., Watanabe, Y., Inaba, Y., and Tajima, K.; Jacc Study Group (2009). Variations in Serum Transforming Growth Factor-β1 Levels with Gender, Age and Lifestyle Factors of Healthy Japanese Adults. Dis. Markers *27*, 23–28. https://doi.org/10.3233/dma-2009-0643.
23. Schmidt, F.M., Weschenfelder, J., Sander, C., Minkwitz, J., Thormann, J., Chittka, T., Mergl, R., Kirkby, K.C., Faßhauer, M., Stumvoll, M., et al. (2015). Inflammatory Cytokines in General and Central Obesity and Modulating Effects of Physical Activity. PLoS One *10*, e0121971. https://doi.org/10.1371/journal.pone.0121971.
24. Yadav, H., Quijano, C., Kamaraju, A.K., Gavrilova, O., Malek, R., Chen, W., Zerfas, P., Zhigang, D., Wright, E.C., Stuelten, C., et al. (2011). Protection from Obesity and Diabetes by Blockade of TGF-β/Smad3 Signaling. Cell Metab. *14*, 67–79. https://doi.org/10.1016/j.cmet.2011.04.013.
25. Massagué, J. (2012). TGFβ signalling in context. Nat. Rev. Mol. Cell Biol. *13*, 616–630. https://doi.org/10.1038/nrm3434.
26. Panday, A., Elango, R., Willis, N.A., and Scully, R. (2022). A modified CUT&RUN-seq technique for qPCR analysis of chromatin-protein interactions. STAR Protoc. *3*, 101529. https://doi.org/10.1016/j.xpro.2022.101529.
27. Noguchi, S., Arakawa, T., Fukuda, S., Furuno, M., Hasegawa, A., Hori, F., Ishikawa-Kato, S., Kaida, K., Kaiho, A., Kanamori-Katayama, M., et al. (2017). FANTOM5 CAGE profiles of human and mouse samples. Sci. Data *4*, 170112. https://doi.org/10.1038/sdata.2017.112.
28. Heldin, C.-H., and Moustakas, A. (2016). Signaling Receptors for TGF-β Family Members. Cold Spring Harb. Perspect. Biol. *8*, a022053. https://doi.org/10.1101/cshperspect.a022053.

29. Hata, A., and Chen, Y.-G. (2016). TGF-β Signaling from Receptors to Smads. Cold Spring Harb. Perspect. Biol. *8*, a022061. https://doi.org/10.1101/cshperspect.a022061.

30. Chielle, E.O., Ogliari, V.C.M., Carvalho, D.d., and Remor, A.P. (2018). Influence of obesity and overweight on transforming growth factor beta 1 levels and other oxidative and cardiometabolic parameters. Clin. Biomed. Res. *38*, 273–280. https://doi.org/10.4322/2357-9730.79449.

31. Pouponnot, C., Jayaraman, L., and Massagué, J. (1998). Physical and Functional Interaction of SMADs and p300/CBP. J. Biol. Chem. *273*, 22865–22868. https://doi.org/10.1074/jbc.273.36.22865.

32. Janknecht, R., Wells, N.J., and Hunter, T. (1998). TGF-β-stimulated cooperation of Smad proteins with the coactivators CBP/p300. Genes Dev. *12*, 2114–2119. https://doi.org/10.1101/gad.12.14.2114.

33. Ghosh, A.K., Yuan, W., Mori, Y., and Varga, J. (2000). Smad-dependent stimulation of type I collagen gene expression in human skin fibroblasts by TGF-β involves functional cooperation with p300/CBP transcriptional coactivators. Oncogene *19*, 3546–3555. https://doi.org/10.1038/sj.onc.1203693.

34. Wakefield, L.M., Winokur, T.S., Hollands, R.S., Christopherson, K., Levinson, A.D., and Sporn, M.B. (1990). Recombinant latent transforming growth factor beta 1 has a longer plasma half-life in rats than active transforming growth factor beta 1, and a different tissue distribution. J. Clin. Investig. *86*, 1976–1984. https://doi.org/10.1172/jci114932.

35. Buenrostro, J.D., Wu, B., Chang, H.Y., and Greenleaf, W.J. (2015). ATAC-seq: A Method for Assaying Chromatin Accessibility Genome-Wide. Curr. Protoc. Mol. Biol. *109*, 21–29. https://doi.org/10.1002/0471142727.mb2129s109.

36. Mikkelsen, T.S., Xu, Z., Zhang, X., Wang, L., Gimble, J.M., Lander, E.S., and Rosen, E.D. (2010). Comparative Epigenomic Analysis of Murine and Human Adipogenesis. Cell *143*, 156–169. https://doi.org/10.1016/j.cell.2010.09.006.

37. Polidori, D., Sanghvi, A., Seeley, R.J., and Hall, K.D. (2016). How Strongly Does Appetite Counter Weight Loss? Quantification of the Feedback Control of Human Energy Intake. Obesity *24*, 2289–2295. https://doi.org/10.1002/oby.21653.

38. Hong, T., Li, J.-Y., Wang, Y.-D., Qi, X.-Y., Liao, Z.-Z., Bhadel, P., Ran, L., Yang, J., Yan, B., Liu, J.-H., and Xiao, X.H. (2021). High Serum Asprosin Levels Are Associated with Presence of Metabolic Syndrome. Int. J. Endocrinol. *2021*, 6622129. https://doi.org/10.1155/2021/6622129.

39. Wang, Y., Qu, H., Xiong, X., Qiu, Y., Liao, Y., Chen, Y., Zheng, Y., and Zheng, H. (2018). Plasma Asprosin Concentrations Are Increased in Individuals with Glucose Dysregulation and Correlated with Insulin Resistance and First-Phase Insulin Secretion. Mediat. Inflamm. *2018*, 9471583. https://doi.org/10.1155/2018/9471583.

40. Kościuszko, M., Buczyńska, A., Duraj, E., Adamska, A., Siewko, K., Krętowski, A.J., and Popławska-Kita, A. (2025). Associations between asprosin, insulin resistance, and oxidative stress in adults with obesity. Sci. Rep. *15*, 40849. https://doi.org/10.1038/s41598-025-24648-7.

41. Uhl, G.R., Martinez, M.J., Paik, P., Sulima, A., Bi, G.-H., Iyer, M.R., Gardner, E., Rice, K.C., and Xi, Z.-X. (2018). Cocaine reward is reduced by decreased expression of receptor-type protein tyrosine phosphatase D (PTPRD) and by a novel PTPRD antagonist. Proc. Natl. Acad. Sci. *115*, 11597–11602. https://doi.org/10.1073/pnas.1720446115.

42. Mishra, I., Duerrschmid, C., Ku, Z., He, Y., Xie, W., Silva, E.S., Hoffman, J., Xin, W., Zhang, N., Xu, Y., et al. (2021). Asprosin-neutralizing antibodies as a treatment for metabolic syndrome. eLife *10*, e63784. https://doi.org/10.7554/elife.63784.

43. Armenise, C., Lefebvre, G., Carayol, J., Bonnel, S., Bolton, J., Di Cara, A., Gheldof, N., Descombes, P., Langin, D., Saris, W.H., et al. (2017). Transcriptome profiling from adipose tissue during a low-calorie diet reveals predictors of weight and glycemic outcomes in obese, nondiabetic subjects. Am. J. Clin. Nutr. *106*, 736–746. https://doi.org/10.3945/ajcn.117.156216.

44. Hinte, L.C., Castellano-Castillo, D., Ghosh, A., Melrose, K., Gasser, E., Noé, F., Massier, L., Dong, H., Sun, W., Hoffmann, A., et al. (2024). Adipose tissue retains an epigenetic memory of obesity after weight loss. Nature *636*, 457–465. https://doi.org/10.1038/s41586-024-08165-7.

45. Campbell, M.K. (2016). Biological, environmental, and social influences on childhood obesity. Pediatr. Res. *79*, 205–211. https://doi.org/10.1038/pr.2015.208.

46. Bouchard, C. (2009). Childhood obesity: are genetic differences involved? Am. J. Clin. Nutr. *89*, S1494–S1501. https://doi.org/10.3945/ajcn.2009.27113c.

47. Ayala, G.X., Monge-Rojas, R., King, A.C., Hunter, R., and Berge, J.M. (2021). The social environment and childhood obesity: Implications for research and practice in the United States and countries in Latin America. Obes. Rev. *22*, e13246–e13350. https://doi.org/10.1111/obr.13350.

48. Williams, D.R., Braddock, A., Houser, M., Blair, G., and Browne, N. (2022). Review of upstream social factors contributing to childhood obesity. Obes. Pillars *4*, 100040. https://doi.org/10.1016/j.obpill.2022.100040.

49. Jia, P., Shi, Y., Jiang, Q., Dai, S., Yu, B., Yang, S., Qiu, G., and Yang, S. (2023). Environmental determinants of childhood obesity: a meta-analysis. Lancet. Glob. Health *11*, S7. https://doi.org/10.1016/s2214-109x(23)00092-x.

50. Letterio, J.J., Geiser, A.G., Kulkarni, A.B., Roche, N.S., Sporn, M.B., and Roberts, A.B. (1994). Maternal Rescue of Transforming Growth Factor-β 1 Null Mice. Science *264*, 1936–1938. https://doi.org/10.1126/science.8009224.

51. Wang, Q.A., Tao, C., Gupta, R.K., and Scherer, P.E. (2013). Tracking adipogenesis during white adipose tissue development, expansion and regeneration. Nat. Med. *19*, 1338–1344. https://doi.org/10.1038/nm.3324.

52. Lu, Y., Yuan, W., Xiong, X., Huang, Q., Chen, S., Yin, T., Zhang, Y., Wang, Z., Zeng, G., and Huang, Q. (2023). Asprosin aggravates vascular endothelial dysfunction via disturbing mitochondrial dynamics in obesity models. Obesity *31*, 732–743. https://doi.org/10.1002/oby.23656.

53. Ulloque-Badaracco, J.R., Al-kassab-Córdova, A., Hernandez-Bustamante, E.A., Alarcon-Braga, E.A., Robles-Valcarcel, P., Huayta-Cortez, M.A., Cabrera Guzmán, J.C., Seminario-Amez, R.A., and Benites-Zapata, V.A. (2024). Asprosin levels in patients with type 2 diabetes mellitus, metabolic syndrome and obesity: A systematic review and meta-analysis. Diabetes Metab. Syndr. *18*, 103095. https://doi.org/10.1016/j.dsx.2024.103095.

54. Morcos, Y.A.T., Lütke, S., Tenbieg, A., Hanisch, F.-G., Pryymachuk, G., Piekarek, N., Hoffmann, T., Keller, T., Janoschek, R., Niehoff, A., et al. (2022). Sensitive asprosin detection in clinical samples reveals serum/saliva correlation and indicates cartilage as source for serum asprosin. Sci. Rep. *12*, 1340. https://doi.org/10.1038/s41598-022-05060-x.

55. Li, E., Shan, H., Chen, L., Long, A., Zhang, Y., Liu, Y., Jia, L., Wei, F., Han, J., Li, T., et al. (2019). OLFR734 Mediates Glucose Metabolism as a Receptor of Asprosin. Cell Metab. *30*, 319–328.e8. https://doi.org/10.1016/j.cmet.2019.05.022.

56. Wei, X., Ao, Q., Meng, L., Xu, Y., Lu, C., Tang, S., Wang, X., and Li, X. (2020). [Expression, purification and functional assessment of asprosin inclusion body]. Nan fang yi ke da xue xue bao J. South. Méd. Univ. *40*, 67–72. https://doi.org/10.12122/j.issn.1673-4254.2020.01.11.

57. Zhang, Y., Zhu, Z., Zhai, W., Bi, Y., Yin, Y., and Zhang, W. (2021). Expression and purification of asprosin in Pichia pastoris and investigation of its increase glucose uptake activity in skeletal muscle through activation of AMPK. Enzyme Microb. Technol. *144*, 109737. https://doi.org/10.1016/j.enzmictec.2020.109737.

58. Yu, Y., He, J.H., Hu, L.L., Jiang, L.L., Fang, L., Yao, G.D., Wang, S.J., Yang, Q., Guo, Y., Liu, L., et al. (2020). Placensin is a glucogenic hormone secreted by human placenta. EMBO Rep. *21*, EMBR201949530. https://doi.org/10.15252/embr.201949530.

59. Mishra, I., Feng, B., Basu, B., Brown, A.M., Kim, L.H., Lin, T., Raza, M.A., Moore, A., Hahn, A., Bailey, S., et al. (2024). The cerebellum modulates thirst. Nat. Neurosci. *27*, 1745–1757. https://doi.org/10.1038/s41593-024-01700-9.

60. Liu, Z., Wang, P., Hu, Y., Zhang, N., Xu, L., Kang, T., Zhao, S., Zhao, D., Chan, C., and Li, J. (2026). Ptprf is the conserved receptor for Asprosin's

glucogenic effects in vertebrates. Cell Rep. *45*, 116974. https://doi.org/10.1016/j.celrep.2026.116974.

61. Hu, Y., Zhao, S., Liu, Z., Kang, T., Hsueh, A.J.W., and Li, J. (2023). Gonacin: A germ cell-derived hormone with glucogenic, orexigenic, and gonadal activities. iScience *26*, 108065. https://doi.org/10.1016/j.isci.2023.108065.
62. Sumithran, P., Prendergast, L.A., Delbridge, E., Purcell, K., Shulkes, A., Kriketos, A., and Proietto, J. (2011). Long-Term Persistence of Hormonal Adaptations to Weight Loss. N. Engl. J. Med. *365*, 1597–1604. https://doi.org/10.1056/nejmoa1105816.
63. Leibel, R.L., Rosenbaum, M., and Hirsch, J. (1995). Changes in Energy Expenditure Resulting from Altered Body Weight. N. Engl. J. Med. *332*, 621–628. https://doi.org/10.1056/nejm199503093321001.
64. Rosenbaum, M., Hirsch, J., Gallagher, D.A., and Leibel, R.L. (2008). Long-term persistence of adaptive thermogenesis in subjects who have maintained a reduced body weight. Am. J. Clin. Nutr. *88*, 906–912. https://doi.org/10.1093/ajcn/88.4.906.
65. Ferreira, R.R., de Souza, E.M., de Oliveira, F.L., Ferrão, P.M., Gomes, L.H.F., Mendonça-Lima, L., Meuser-Batista, M., Bailly, S., Feige, J.J., de Araujo-Jorge, T.C., and Waghabi, M.C. (2016). Proteins involved on TGF-β pathway are up-regulated during the acute phase of experimental Chagas disease. Immunobiology *221*, 587–594. https://doi.org/10.1016/j.imbio.2016.01.009.
66. Wang, B., Dileepan, T., Briscoe, S., Hyland, K.A., Kang, J., Khoruts, A., and Cleary, P.P. (2010). Induction of TGF-β1 and TGF-β1–dependent predominant Th17 differentiation by group A streptococcal infection. Proc. Natl. Acad. Sci. *107*, 5937–5942. https://doi.org/10.1073/pnas.0904831107.
67. Sarahrudi, K., Thomas, A., Mousavi, M., Kaiser, G., Köttstorfer, J., Kecht, M., Hajdu, S., and Aharinejad, S. (2011). Elevated transforming growth factor-beta 1 (TGF-β1) levels in human fracture healing. Injury *42*, 833–837. https://doi.org/10.1016/j.injury.2011.03.055.
68. Singh, M., Orazulike, N.C., Ashmore, J., and Konje, J.C. (2013). Changes in Maternal Serum Transforming Growth Factor Beta-1 during Pregnancy: A Cross-Sectional Study. BioMed Res. Int. *2013*, 318464. https://doi.org/10.1155/2013/318464.
69. Pasarica, M., Shin, A.C., Yu, M., Ou Yang, H.M., Rathod, M., Jen, K.L.C., MohanKumar, S., MohanKumar, P.S., Markward, N., and Dhurandhar, N.V. (2006). Human Adenovirus 36 Induces Adiposity, Increases Insulin Sensitivity, and Alters Hypothalamic Monoamines in Rats. Obesity *14*, 1905–1913. https://doi.org/10.1038/oby.2006.222.
70. Atkinson, R.L., Dhurandhar, N.V., Allison, D.B., Bowen, R.L., Israel, B.A., Albu, J.B., and Augustus, A.S. (2005). Human adenovirus-36 is associated with increased body weight and paradoxical reduction of serum lipids. Int. J. Obes. *29*, 281–286. https://doi.org/10.1038/sj.ijo.0802830.
71. Gabbert, C., Donohue, M., Arnold, J., and Schwimmer, J.B. (2010). Adenovirus 36 and Obesity in Children and Adolescents. Pediatrics *126*, 721–726. https://doi.org/10.1542/peds.2009-3362.
72. Li, D.-K., Chen, H., Ferber, J., and Odouli, R. (2020). Maternal infection and antibiotic use in pregnancy and the risk of childhood obesity in offspring: a birth cohort study. Int. J. Obes. *44*, 771–780. https://doi.org/10.1038/s41366-019-0501-2.
73. Ginkel, A.C.P., Wijga, A.H., Bruijning-Verhagen, P.C.J., Brunekreef, B., Gehring, U., Hoek, W. van der, Koppelman, G.H., Rossem, L. van, Sande, M.A.B. van der, and Smit, H.A. (2021). Early childhood infections and body mass index in adolescence. Int. J. Obes. *45*, 1143–1151. https://doi.org/10.1038/s41366-021-00806-5.
74. Moffat, J., Grueneberg, D.A., Yang, X., Kim, S.Y., Kloepfer, A.M., Hinkle, G., Piqani, B., Eisenhaure, T.M., Luo, B., Grenier, J.K., et al. (2006). A Lentiviral RNAi Library for Human and Mouse Genes Applied to an Arrayed Viral High-Content Screen. Cell *124*, 1283–1298. https://doi.org/10.1016/j.cell.2006.01.040.
75. STEWART, S.A., DYKXHOORN, D.M., PALLISER, D., MIZUNO, H., YU, E.Y., AN, D.S., SABATINI, D.M., CHEN, I.S.Y., HAHN, W.C., SHARP, P.A., et al. (2003). Lentivirus-delivered stable gene silencing by RNAi in primary cells. RNA *9*, 493–501. https://doi.org/10.1261/rna.2192803.
76. Langmead, B., and Salzberg, S.L. (2012). Fast gapped-read alignment with Bowtie 2. Nat. Methods *9*, 357–359. https://doi.org/10.1038/nmeth.1923.
77. McLean, C.Y., Bristor, D., Hiller, M., Clarke, S.L., Schaar, B.T., Lowe, C.B., Wenger, A.M., and Bejerano, G. (2010). GREAT improves functional interpretation of cis-regulatory regions. Nat. Biotechnol. *28*, 495–501. https://doi.org/10.1038/nbt.1630.
78. Feng, J., Liu, T., Qin, B., Zhang, Y., and Liu, X.S. (2012). Identifying ChIP-seq enrichment using MACS. Nat. Protoc. *7*, 1728–1740. https://doi.org/10.1038/nprot.2012.101.
79. Zebisch, K., Voigt, V., Wabitsch, M., and Brandsch, M. (2012). Protocol for effective differentiation of 3T3-L1 cells to adipocytes. Anal. Biochem. *425*, 88–90. https://doi.org/10.1016/j.ab.2012.03.005.
80. Ratnadiwakara, M., and Änkö, M.L. (2018). mRNA Stability Assay Using transcription inhibition by Actinomycin D in Mouse Pluripotent Stem Cells. Bio. Protoc. *8*, e3072. https://doi.org/10.21769/bioprotoc.3072.
81. Gui, X., Deng, M., Song, H., Chen, Y., Xie, J., Li, Z., He, L., Huang, F., Xu, Y., Anami, Y., et al. (2019). Disrupting LILRB4/APOE Interaction by an Efficacious Humanized Antibody Reverses T-cell Suppression and Blocks AML Development. Cancer Immunol. Res. *7*, 1244–1257. https://doi.org/10.1158/2326-6066.cir-19-0036.
82. Mishra, I., and Chopra, A.R. (2022). Overexpression and ELISA-based detection of asprosin in cultured cells and mice. STAR Protoc. *3*, 101762. https://doi.org/10.1016/j.xpro.2022.101762.
83. Bray, N.L., Pimentel, H., Melsted, P., and Pachter, L. (2016). Erratum: Near-optimal probabilistic RNA-seq quantification. Nat. Biotechnol. *34*, 888. https://doi.org/10.1038/nbt0816-888d.
84. Robinson, M.D., McCarthy, D.J., and Smyth, G.K. (2010). edgeR: a Bioconductor package for differential expression analysis of digital gene expression data. Bioinformatics *26*, 139–140. https://doi.org/10.1093/bioinformatics/btp616.
85. Ramírez, F., Dündar, F., Diehl, S., Grüning, B.A., and Manke, T. (2014). deepTools: a flexible platform for exploring deep-sequencing data. Nucleic Acids Res. *42*, W187–W191. https://doi.org/10.1093/nar/gku365.

STAR★METHODS

KEY RESOURCES TABLE

REAGENT or RESOURCE	SOURCE	IDENTIFIER
Antibodies		
Mouse anti-asprosin	Mishra et al., 2022[15]	N/A
Human anti-asprosin	This paper	N/A
Goat anti-mouse HRP	Tonbo Biosciences	Cat# 72-8042-M001; RRID: AB_3750732
Rabbit anti-asprosin	This paper	N/A
Anti-H3K27Ac antibody	Abcam	Cat# ab4729; RRID: AB_2118291
Mouse IgG control	SouthernBiotech	Cat# 0107-01; RRID: AB_2732898
Bacterial and virus strains		
pAAV-mTGFB1	This paper	N/A
pLenti-mTGF-β1	Origene	Cat# MR227339L4
pLKO.1-TRC	Addgene (Moffat et al., 2006)[74]	Cat# 10878
AAV8-empty	This paper	N/A
AAV8-IL2-asprosin	This paper	N/A
Chemicals, peptides, and recombinant proteins		
Recombinant Mouse TGF-β1 (carrier-free)25ug	Biolegend	Cat# 763104
Recombinant leptin	Novus Biologicals	Cat# 103685-244
Tamoxifen	Sigma-Aldrich	Cat# T5648
Corn Oil	Sigma-Aldrich	Cat# C8267
ITSA-1	Sigma-Aldrich	Cat# I7152
A-485	MedChemExpress	Cat# HY-107455
7-BIA	Tocris	Cat# 6310
Recombinant Mouse IFN-γ	Biolegend	Cat# 575302
Recombinant Mouse IL-1B	Biolegend	Cat# 575102
Recombinant Mouse IL-6	Biolegend	Cat# 575702
Recombinant Mouse TNF-α	Biolegend	Cat# 575202
Dexamethasone	Cayman Chemical Company	Cat# 11015
IBMX	Cayman Chemical Company	Cat# 13347
Insulin	Sigma-Aldrich	Cat# I9278
Rosiglitazone	Cayman Chemical Company	Cat# 71740
Puromycin	Sigma-Aldrich	Cat# P9620
Actinomycin D	Thermo Fisher Scientific	Cat# 11805017
Recombinant Mouse Asprosin	Biolegend	Cat# 762002
Critical commercial assays		
DNA purification kit	Monarch	Cat# T3010S
TGF-β1 ELISA	R&D Systems	Cat# DY1679
RNeasy kit	Qiagen	Cat# 74106
Lenti-X Concentrator	Takara	Cat# 631231
NEBNext rRNA Depletion Kit v2	New England Biolabs	Cat# E7400
NEBNext Ultra II Directional RNA Library Prep kit	New England Biolabs	Cat# E7760
ATAC-seq kit	Active Motif	Cat# 53150
Qiagen Qiaquick Gel Extraction kit	Qiagen	Cat# 28704
CUT&Tag-IT Tissue Kit	Active Motif	Cat# 53170

(*Continued on next page*)

Continued

REAGENT or RESOURCE	SOURCE	IDENTIFIER
Deposited data		
Raw and Analyzed Data	This paper	GEO: GSE277913 and GSE277916
Re-analysis of Adipose Tissue Epigenetic Memory	Hinte et al., 2024[44]	GEO: GSE236578
Re-analysis of Human FBN1 mRNA	Armenise et al., 2017[43]	GEO: GSE95640
Experimental models: Cell lines		
Mouse: 3T3-L1	ATCC	Cat# CL-173; RRID:CVCL_0123
HEK293T	ATCC	Cat# CRL-3216; RRID:CVCL_0063
Experimental models: Organisms/strains		
C57BL/6J Mus musculus	Jackson Laboratory	Cat# JAX:000664; RRID:IMSR_JAX:000664
C57BL/6J DIO Mus musculus (males)	Jackson Laboratory	Cat# JAX: 380050; RRID:IMSR_JAX:380050
C57BL/6- C57BL/6-*Fbn1*$^{em1Chop/J}$ Mus musculus	Jackson Laboratory	Cat# JAX: 033548; RRID:IMSR_JAX:033548
FVB/NJ Mus musculus	Jackson Laboratory	Cat# JAX: 001800; RRID:IMSR_JAX:001800
B6.Cg-Lep^{ob}/J Mus musculus	Jackson Laboratory	Cat# JAX: 000632; RRID:IMSR_JAX:000632
C57BL/6J DIO Mus musculus (females)	This paper	N/A
C57BL/6-Tg (Adipoq-icre/ERT2)1Soff/J	Jackson Laboratory	CAT# JAX: 025124; RRID:IMSR_JAX:025124
C57BL/6J *Fbn1* exon 66$^{flx/flx}$	This paper	
Oligonucleotides		
Primers For Guide Sequences for pLKO.1 (see Table S2)	This paper	N/A
Primer for Adipoq-iCre+/*Fbn1* exon 66$^{flx/flx}$ Forward: 5′ GAGGCCTGCTATGAGTGTAAG 3′	This paper	N/A
Primer for Adipoq-iCre+/*Fbn1* exon 66$^{flx/flx}$ Reverse: 5′ GAGAAGCCTGAGAAAGTGGTT 3′	This paper	N/A
Primers for qPCR (see Table S3)	This paper	N/A
Recombinant DNA		
psPAX2	Addgene (Didier Trono Lab)	Cat# 12260
pCMV-VSV-G	Addgene (Stewart et al., 2003)[75]	Cat# 8454
Software and algorithms		
Graphpad Prism version 10	GraphPad	https://www.graphpad.com
R version 4.0.3	R software	https://www.R-project.org
Illumina's CASAVA 1.8.2	Illumina	http://www.illumina.com
Trim Galore! V 0.6.7	Felix Krueger lab	https://www.bioinformatics.babraham.ac.uk/projects/trim_galore/
Bowtie2 v 2.4.5	Langmead and Salzberg, 2013[76]	http://bowtie-bio.sourceforge.net/bowtie2/index.shtml
Picard MarkDuplicates v2.18.2.3	Broad Institute	http://broadinstitute.github.io/picard/
Deeptools v3.4.3	Mclean et al., 2010[77]	N/A
MACS2 v2.2.7.1	Feng et al., 2012[78]	http://liulab.dfci.harvard.edu/MACS
DiffBind v2.10.0	Bioconductor	http://bioconductor.org/packages/release/bioc/html/DiffBind.html
Other		
Teklad High Fat Diet	Envigo	Cat# TD.06414
Dustless Pellet Diet	Bio-Serv	Cat# F0172

(*Continued on next page*)

Continued

REAGENT or RESOURCE	SOURCE	IDENTIFIER
Trackit 1Kb Plus DNA Ladder	Thermo Fisher Scientific	Cat# 10488085
EDTA Coated Tubes	BD Microtainer	Cat# 365974
SYBR Green PCR Master Mix	Thermo Fisher	Cat# 4367659
Fugene HD	Promega	Cat# E2311

EXPERIMENTAL MODEL AND STUDY PARTICIPANT DETAILS

Mice

Wild-type C57BL/6 mice (WT mice; JAX# 000664), C57BL/6J DIO (JAX# 380050), *Fbn1*$^{NPS/+}$ (C57BL/6- C57BL/6-*Fbn1*$^{em1Chop/J}$; JAX# 033548), B6.Cg-Lep^{ob}/J (JAX# 000632) and FVB/NJ (JAX# 001800) were purchased from The Jackson Laboratory (JAX).

To generate DIO female mice, 3 week old female WT C57BL/6 mice were purchased from JAX and put on Teklad HFD (60% fat, TD.06414, Envigo) for 6 months. During this time, they were mated with males twice to ensure they were capable of producing viable pups, but those pups were not used in this study. Only after the female mice had been on HFD for 6 months, they were bred with new 12-week-old WT male mice, and these were the pups used for the study. For the TGF-β1 injection study, 9 week old female FVB/NJ mice were purchased from the Jackson Laboratory and mated with 12 week old WT male mice.

Age- and sex-matched littermates from in-house mating served as controls in all experiments, except for WT mice without obesity and DIO mice that were bought from the Jackson Laboratory and used for experimentation after acclimation to the mouse housing facility. Mice were housed in micro-ventilator cages on a 12-h light cycle in animal facility maintained at 20°C–25°C and 40–60% humidity. Mice had *ad-libitum* access to water and normal chow (5V5R, lab Supply), Teklad high fat diet (TD.06414, Envigo), or dustless pellet diet (F0172, Bio-Serv), unless otherwise specified.

Animal housing, husbandry, and euthanasia were conducted under animal protocols approved by the Case Western Reserve University Institutional Animal Care and Use Committee (protocol# 2018-0042). General health of mice was monitored by the CWRU animal resource center.

Inducible, adipocyte-specific *Fbn1* knockout mouse line

A conditional floxed mouse line was generated using Cyagen Biosciences' ES microinjection and germline F1 breeding platform (BCM001_mFbn1_1A12). Briefly, *loxP* sites were inserted flanking exon 66 of *Fbn1* (exon 66 encodes 129 of the 140 amino acids that comprise the asprosin protein), and homozygous floxed (*Fbn1* exon 66$^{flx/flx}$) mice were established. These mice were then crossed with *Adipoq*-iCreERT2 transgenic mice (C57BL/6-Tg (Adipoq-icre/ERT2)1Soff/J, JAX #:025124) in which expression of a tamoxifen-inducible, codon-improved Cre recombinase (iCreERT2) is restricted to mature adipocytes under the *Adipoq* promoter. The resulting *Adipoq*-iCre; *Fbn1* exon 66$^{flx/flx}$ mice enabled adipocyte-specific deletion of asprosin only after the administration of tamoxifen. To induce recombination, male mice (4–6 weeks of age, post-weaning) were injected intraperitoneally with tamoxifen (100 mg/kg body weight dissolved in corn oil) (Sigma-Aldrich, T5648) once daily for 5 consecutive days. Littermate *Fbn1* exon 66$^{flx/flx}$ mice lacking iCre (Adipoq-iCre-; *Fbn1* exon 66$^{flx/flx}$) or littermate iCre mice lacking floxed allele (Adipoq-iCre+; *Fbn1*$^{+/+}$) were injected with tamoxifen and used as controls. In some cases, mice with *Adipoq*-Cre; *Fbn1* exon 66$^{flx/flx}$ were injected with oil instead of tamoxifen (recombination not induced) and used as controls. To control for potential confounding from tamoxifen-induced metabolic effects, and consistent with prior studies employing CreERT2 systems, we incorporated a minimum three-week tamoxifen washout before initiating diet changes or other analyses.

Mice were sacrificed and brain, heart, liver, skeletal muscle, perigonadal and subcutaneous adipose tissues were collected. Genomic DNA was made from these tissues using genomic DNA purification kit (Monarch; #T3010S) and DNA was PCR amplified on a thermocycler using the following primers: Forward primer: 5′ GAGGCCTGCTATGAGTGTAAG 3'; Reverse primer: 5′ GAGAAGCCTGAGAAAGTGGTT 3'. Amplified PCR products with invitrogen trackit 1 Kb Plus DNA Ladder (Thermo Fisher Scientific; 10488085) were run on a 1% agarose gel for 60 min. Nucleic acid gel was visualized using Invitrogen iBright Imagers.

Cell lines and reagents

Cell lines were incubated at 37°C with 5% CO_2 under humidified conditions. 3T3-L1 cells (CL-173) were purchased from ATCC. Cells were authenticated via ATCC STR profiling and were routinely tested for mycoplasma contamination using a PCR-based detection assay. Mouse recombinant carrier-free TGF-β1 (763104), IFN-γ (575302), IL-1B (575102), IL-6 (575702), TNF-α (575202) were all purchased from Biolegend. A-485 (HY-107455) was purchased from MedChemExpress. pLenti-mTGF-β1 (MR227339L4) was purchased from Origene.

METHOD DETAILS

Alternate day fasting

The alternate day fasting design was identical for the partial (10%) and complete (25%) weight-loss groups, differing only in the total duration of the protocol. DIO mice maintained on an HFD were transferred to clean cages and fasted for approximately 18 h (overnight) with *ad libitum* access to water. The following day, standard chow was reintroduced, and mice were allowed to feed freely for 24 h. This fasting–refeeding cycle was repeated for 2 weeks for the partial weight loss (10%) cohort. For the complete weight loss (25%) cohort, the same fasting–refeeding cycle was extended to 3.5 weeks, followed by a three-day recovery period on normal chow. An average reduction in body weight of 25% over a 3.5-week alternate day fasting protocol was enough to achieve the same body weight as age- and sex-matched control mice without prior obesity.

At the conclusion of both the two-week regimen or 3.5-week regimen, all mice were maintained on normal chow for three consecutive days without fasting to eliminate residual metabolic effects of the overnight fast.

The experimental design for *ob/ob* mice was identical to that described above, except that the total duration was 12 days. On each refeeding day, mice received an IP injection of 15 μg recombinant leptin (Novus Biologicals, #103685-244) per animal.

In-vivo cytokine treatment

Recombinant mouse TGF-β1 (R&D Systems, #7666-B2-010) was diluted in sterile PBS and injected IP at 0.5 μg per mouse twice daily for 4 days. Vehicle control mice received equivalent volumes of PBS injections.

Plasma was collected via submandibular bleed into EDTA-coated tubes (BD Microtainer #365974), centrifuged at 1,500 × *g* for 15 min at 4°C, and stored at −80°C until analysis. Total and active TGF-β1 were quantified by ELISA (R&D Systems #DY1679) following acid activation per the manufacturer's instructions.

Pharmacologic interventions and inhibitor treatments

For *in-vivo* histone-modifying interventions, the small-molecule HDAC activator ITSA-1 (Sigma-Aldrich #I7152) was administered IP at 4 mg/kg per day for 5 days, followed by 1 day of rest. Mice were then cheek-bled the next day, given an additional day of rest, and then subsequently placed on *ad libitum* HFD for 13 days. For *in vitro* experiments, differentiated 3T3-L1 adipocytes were treated with 20 ng/mL TGF-β1 for 4 days. Following treatment, cells were washed three times with PBS and subsequently incubated with 100 μM ITSA-1 for an additional 3 days prior to downstream assays.

For inhibition of the p300/CBP acetyltransferase, differentiated 3T3-L1 adipocytes were pretreated with either DMSO or 100 nM A-485 (MedChemExpress #HY-107455) in complete medium for 6 h. Subsequently, cells were treated with 20 ng/mL TGF-β1 in combination with either DMSO or 100 nM A-485 and incubated for an additional 4 days prior to analysis.

For blockade of Ptprd signaling, mice received 7-BIA (Tocris #6310) daily by intraperitoneal injection at 150 μg or 300 μg (for ob/ob mice with partial weight loss (10%)) or 150 μg for all other experiments.

For asprosin neutralization, a validated monoclonal mouse anti-asprosin antibody (5.55 μg/g body weight per day) or isotype-matched IgG was delivered intraperitoneally.

TGF-β1 injection into FVB/NJ females

9-week-old female FVB/NJ mice were mated with 12-week-old WT male mice or 12-week-old *Fbn1*$^{NPS/+}$ mice. Time of pregnancy was noted by observation of vaginal plug and exactly 14 days later, subcutaneous injections started. Specifically, 2.5 μg of recombinant TGF-β1 (Biolegend, 763104) was injected twice daily [morning (8-9am) and afternoon (4-5pm)] made up in 100 μl of sterile USP-grade saline for about 7 days or until the females gave birth. The pups were weaned and placed on normal chow.

Metabolic caging and food intake assessment

Metabolic caging experiments were performed at the Cardiovascular Research Institute Mouse Metabolic and Phenotyping Core at CWRU (IACUC# 2019-0029). Mice were housed with a 12-h light/dark cycle (7am/7pm) at 22°C with controlled humidity. Metascreen software (V2.3.15.11) controlled system data acquisition. Respirometry (VO_2, VCO_2) were collected individually using a Promethion metabolic cage system (Sable Systems, Las Vegas, NV, USA). Gas analyzers were calibrated before each run. Gas measurements were multiplexed over 8 cages and baselined to a cage-equivalent volume of room air twice per 5-min cycle, while maintaining a 2L/min/cage, negative pressure-derived flow rate. Acquired data was processed using Macro Interpreter (V2.34) running Macro V2.33.3-slice1hr. Energy expenditure was calculated using the Weir equation (Weir, 1949).

For manual food intake measurements, mice were acclimated to dustless pellet diet (F0173, Bio-Serv) for three days in single-housing, after which the 24 h food intake was measured. For the pups from TGF-β1 injected female manual food intake, the mice were acclimated to a crushed high fat diet formed into a ball (60% calories from fat, TD.06414, Envigo Teklad) in single housing for three days.[79] The diet was replenished, weighed, and re-weighed to establish a 24-h food intake.

Differentiation of 3T3-L1 cells

The differentiation protocol of 3T3-L1 cells used was one previously published utilizing a cocktail consisting of IBMX, rosiglitazone, insulin, and dexamethasone.[74] Briefly, undifferentiated 3T3-L1 cells were plated into 12-well plates at 0.8x10^5 cells/well. Cells were

grown to 100% confluency and 48 h later, a cocktail of differentiation media [High Glucose DMEM, 10% FBS, 1uM Dexamethasone (Cayman Chemical Company, 11015), 0.5mM IBMX (Cayman Chemical Company, 13347), 10 μg/mL Insulin (Sigma-Aldrich, I9278), 30uM Rosiglitazone(Cayman Chemical Company, 71740)] was added for 48 h. Then the media was changed to a maintenance media (High Glucose DMEM, 10% FBS, 10 μg/mL Insulin) and kept for 5 days.

shRNA knockdown

For shRNA knockdown of genes, the pLKO.1-TRC lentiviral cloning vector was utilized following Addgene's protocol (10878, Addgene) previously reported.[80] Specifically, short-hairpin constructs targeting Tgfbr2 and Smad4 were cloned into pLKO.1. For controls, the empty vector was utilized. The packaging vectors used to generate lentiviral particles were psPAX2 (12260, Addgene) and pCMV-VSV-G (8454, Addgene) that were transfected into HEK293T (ATCC, CRL-3216) cells using Fugene HD (Promega, E2311). 48 h later, viral particles were collected and concentrated using Lenti-X Concentrator (Takara, 631231) and filtered through 0.45 μm PES filters. Differentiated 3T3-L1 cells were transduced at 80% confluence for 24 h and selected with 2 μg/mL puromycin (Sigma #P9620) for 3 days. Cells were then treated with 20 ng/mL TGF-β1 for 48 h before RNA isolation. Knockdown efficiency was validated by qPCR. The sequences of primers used to target each gene are provided (Table S2). Furthermore, 3 different viruses targeting 3 different guide sequences to the same gene were pooled and all transduced to a single sample of cells to maximize knock-down efficacy.

Quantitative PCR

For cell culture work, *Smad7* and *FBN1* expression was measured in differentiated 3T3-L1 cells. For *in-vivo* tissue, white adipose tissue (visceral perigonadal adipose tissue unless stated otherwise) was excised from mice. Aliquots of these tissues weighing 0.3 grams and cells were used for RNA extraction using the RNeasy kit (Qiagen) following manufacturer's instructions. For adipose tissue, a tissue homogenizer was utilized. First strand cDNA was synthesized with Iscript™ cDNA synthesis kit (Bio-Rad) and subjected to qPCR analysis.

Real-time qPCR was performed using Power SYBR™ Green PCR Master Mix (Thermo Fisher) and the Bio-Rad CFX96 Real-Time system (Bio-Rad). Sequence of primers used are provided (Table S3).

Specifically for assessing additional transcription start sites on the *FBN1* gene specific for asprosin, more primer sets were utilized against *FBN1*, the primer set listed above was the 'Asprosin' primer set as depicted in the figure. The sequence of the other two primer sets are provided (Table S3).

mRNA half-life

20 ng/mL of recombinant mouse TGF-β1 was added to differentiated 3T3-L1 cells. 24 h later, 30 μg/mL actinomycin D (Thermo Fisher Scientific, 11805017) was added. RNA was collected at 0, 1, 6, 12, and 24 h post addition of actinomycin D and purified using RNeasy Mini Kit (Qiagen). Half-life was determined using a previously published method,[81] specifically using quantitative PCR with primers against *FBN1*. A one phase decay non-linear fit model was used to determine half-life.

Asprosin ELISA

A custom-built sandwich ELISA was used for measuring plasma, serum, and media asprosin. For plasma and serum asprosin, 25uL plasma or serum (plus 75ul PBS) was captured using a fully human anti-asprosin monoclonal antibody (human anti-asprosin mAb), previously generated from a naive human phage display antibody library by panning against recombinant full-length human asprosin (Texas Therapeutics Institute at the University of Texas Health Science Center at Houston). A mouse anti-asprosin monoclonal antibody (mouse anti-asprosin mAb), against human asprosin amino acids 106–134 (human profibrillin amino acids 2838–2865) served as the detection antibody. An anti-mouse secondary antibody linked to HRP was used to generate a signal, and mammalian-cell produced recombinant mouse asprosin (Biolegend 762002) was used to generate a standard curve.

For the media asprosin ELISA, 100 μl of media was used. In this protocol, the mouse anti-asprosin mAb served as the capture antibody, and a fully rabbit anti-asprosin mAb (RevMAb) served as the detection antibody, which was generated by immunizing rabbits with recombinant full-length human asprosin at RevMAb Biosciences, USA, and cloning variable region genes from positive single memory B cells based on protocols described previously.[14,15,42,82] An anti-rabbit secondary antibody linked to HRP was used to generate a signal. Because plasma and media protocols use different antibody configurations, absolute values between the two assays were not compared to one another and were not compared across experiments. All ELISAs were used exclusively to assess within-experiment, directional changes. Across all plasma ELISAs, individual lean animals span approximately 1–8 nM, which reflects normal biological scatter for a circulating hormone; the modest difference in lean means between cohorts of different ages lies within this range and reflects age and cohort differences rather than assay variability. All mechanistic conclusions were based on relative differences between matched control and experimental animals run side-by-side on the same plate, not on cross-experiment comparisons of absolute nM values.

Adeno-associated virus injection

Six 14-week-old normal chow fed female WT C57BL/6 from JAX were injected intravenously via the tail-vein with adeno-associated virus (AAV) serotype 8 as previously described dissolved in 150 μL USP-grade sterile saline.[83] Mice injected with AAV8-empty

(1×10^{12} GC/mouse) served as controls for experimental mice that received AAV8-IL2-asprosin (1×10^{12} GC/mouse) containing an N-terminal his-tagged human asprosin coding region preceded by an IL2 signal peptide, under control of an EF1 promoter. 5 weeks after injection, plasma was collected via cheek bleed. The injected females were then set up for matings with 12-week-old WT males.

RNA sequencing

Fully differentiated 3T3-L1 cells were incubated with PBS, recombinant TGF-β1 for 4 days, or recombinant TGF-β1 for 4 days plus an additional 14 days in TGF-β1 free media. Total RNA was extracted using RNeasy Mini Kit (Qiagen #74106). Quality control of total RNA samples was executed using Qubit Fluorometer (Invitrogen) for RNA quantification and Fragment Analyzer 5200 (Agilent) to assess RNA quality using a cut-off of RIN >7.0 to select specimens for further analysis. The NEBNext rRNA Depletion Kit v2 (Human/Mouse/Rat) (New England Biolabs) was completed first. The rRNA-depleted RNA was used as input for the NEBNext Ultra II Directional RNA Library Prep kit for Illumina (New England BioLabs) in which libraries were tagged with unique adapter-indexes. Final libraries were validated on the Fragment Analyzer, quantified via qPCr, and pooled at equimolar ratios. Pooled libraries were diluted, denatured and loaded onto the Illumina NextSeq 550 sequencing system, following the Illumina User Guide for a single read run. To analyze gene expression changes, reads were aligned to the mm10 genome build using kallisto v0.46.1.[84] The transcripts were quantified in TPM, which was further processed into gene-level TPM abundance using tximport. Differential gene expression analysis was conducted using edgeR v3.36.0,[85] and significant genes were called based on an adjusted p value of less than 0.05 with a $\log_2$ (FC) greater than 1. Gene set enrichment analysis was generated from the c2.cp.keg database using 1,000 permutations.

ATAC sequencing

Fully differentiated 3T3-L1 cells were incubated with PBS, recombinant TGF-β1 for 4 days, or recombinant TGF-β1 for 4 days plus an additional 14 days in TGF-β1 free media. Samples were prepared following protocol provided at ATAC-seq kit (Active Motif #53150). Samples were run on an E-Gel EX 2% Agarose gel (Thermo Fisher Scientific) prior to manual size selection for fragments less than 1000bp and extraction was done using the Qiagen Qiaquick Gel extraction kit (Qiagen, 28704). Insert size distribution was determined with an Agilent TapeStation assay and samples were quantified by qPCR using a commercially available kit (KAPA Biosystems). Sample concentrations were normalized to 1.2nM and loaded onto an Illumina NovaSeq flow cell at a concentration that yields 50 million passing filter clusters per sample. Samples were sequenced using 150bp paired-end sequencing on an Illumina NovaSeq according to Illumina protocols. The 8bp unique dual index was read during additional sequencing reads that automatically follow the completion of read1. Data generated during the sequencing runs are simultaneously transferred to the YCGA high-performance computing cluster. A positive control (prepared bacteriophage Phi X library) provided by Illumina was spiked into every lane at a concentration of 0.3% to monitor sequencing quality in real time. Signal Intensities were converted to individual base calls during a run using the system's Real Time Analysis (RTA) software. Base calls were transferred from the machine's dedicated personal computer to the Yale High Performance Computing cluster via a 1 Gigabit network mount for downstream analysis. Primary analysis - sample de-multiplexing and alignment to the mouse genome - was performed using Illumina's CASAVA 1.8.2 software suite. The data was returned to the user if the sample error rate is less than 2% and the distribution of reads per sample in a lane is within reasonable tolerance.

CUT&Tag sample preparation

Subcutaneous adipose tissue from 15 week old mice born to dams injected with PBS or TGF-B1 were obtained. The samples were processed using the Active Motif CUT&Tag-IT Tissue kit (Active Motif, 53170) according to the manufacturer's instructions. Briefly nuclei were extracted from tissue using kit lysis buffer and douce homogenizer and filtered using 40μm strainer. The samples were incubated with an antibody targeting H3K27Ac (abcam, ab4729). After incubation, Protein A-Tn5 was added for DNA cleavage and tagmentation. The cleaved DNA fragments were isolated, amplified, and sequenced on the Illumina NextSeq to 10 million paired-end reads per sample.

Peak calling and analysis

Raw reads from ATAC-seq and CUT&Tag were quality and adaptor trimmed using Trim Galore! version 0.6.7 (https://www.bioinformatics.babraham.ac.uk/projects/trim_galore/). Trimmed reads were then aligned to the mm10 genome build using bowtie2 version 2.4.5. Duplicate reads were filtered using Picard MarkDuplicates version 2.18.2.3 (http://broadinstitute.github.io/picard/). Reads per genome coverage (RPGC)- normalized bigWig and bedgraph files were generated using the bamcoverage functions in deeptools version 3.4.3.[77] Peaks were called using MACS2 version 2.2.7.1 using a qvalue cutoff of 0.001.

Diffbind analysis

PBS added (control), TGF-β1 activated for 4 days, and TGF-β1 activated plus an additional 14 days in TGF-β1 free media ATAC-sequencing and CUT&Tag was performed in duplicate (triplicate for the Free condition). Differential binding analysis between the groups was performed using Diffbind package version 2.10.0 (http://bioconductor.org/packages/release/bioc/html/DiffBind.html). Peak-gene assignments, Gene Ontology analysis, and peak location distribution were analyzed using GREAT.[77] Functional peaks were defined according to differentially expressed genes obtained from transcriptomic analysis ($\log_2$FC > 1 between Tgf- β1 versus

control). For ATAC sequencing, heat maps of chromatin accessibility were generated using the computeMatrix and plotHeatmap functions in deeptools (v3.5.3). For these heat maps, RPGC-normalized bigWig files were used as the score files and the peaks that were increased by at least 4-fold on Diffbind with Tgf-β1 treatment were used as the input region file.

In vivo anti-asprosin mAb treatment

Mice were acclimated to metabolic cages with *ad libitum* HFD and water for 2 days before the experiment. Mice were injected IP with either an anti-asprosin mAb or a mouse IgG control antibody (5.5 μg/g mouse weight in 150ul USP-grade saline per mouse). For both the DIO mice experiments and the dams with PBS/TGF-β1 injection experiment, antibody injections were daily from 3 to 4 pm for 14 days.

Third party independent validation

Independent third-party validation experiments were conducted by Kyle Starost and Natalia Aladyshkina in the Seth Field lab at the Harrington Discovery Institute at University Hospitals. All experiments strictly followed the protocol described in this manuscript to reproduce the results shown in Figures 2A–2C,F,I.

QUANTIFICATION AND STATISTICAL ANALYSIS

All quantitative data are expressed as mean ± standard error of the mean (s.e.m.) unless otherwise specified. Statistical analyses were performed using GraphPad Prism v9 or higher. The choice of statistical test was determined by the experimental design and data distribution. For comparisons between two independent groups, unpaired two-tailed Student's *t*-tests were used. Two-sided t-tests were used unless a specific directional hypothesis was established *a priori*, in which case one-sided t-tests were used. For experiments involving more than two groups or multiple independent variables, one-way or two-way analyses of variance (ANOVA) were conducted, respectively. When ANOVA indicated a significant main effect or interaction, Bonferroni's post hoc multiple-comparison tests were applied to identify specific group differences. Repeated-measures ANOVA was employed for datasets in which multiple measurements were obtained from the same animals over time, accounting for within-subject variability. All mice were randomly assigned to experimental groups, with age and sex balanced across conditions to minimize biological bias. Investigators were blinded to group allocation during data collection and analysis for Promethion metabolic data, quantitative PCR (qPCR) assays, and sandwich ELISA measurements. The number of biological replicates (n) for each experiment is indicated in the corresponding figure legends. For all cell culture experiments, each biological replicate consisted of 2 technical replicates. An alpha level (α) of 0.05 was set as the threshold for statistical significance.

All mice, whether bred in-house or obtained from Jackson Laboratory, were randomly assigned to experimental or control groups without prior body weight stratification. Because natural variation exists among age- and sex-matched mice, minor differences in baseline weights may have occurred. Accordingly, statistical analyses and interpretations were based on body weight change rather than absolute values. For transparency, raw body weights and their corresponding statistical analyses are provided in the Supplemental Figures.